INVESTIGATION OF A NOVEL COMPACT VIBRATION ISOLATION SYSTEM FOR SPACE APPLICATIONS

THESIS

Steven D. Miller, Second Lieutenant, USAF

AFIT/GA/ENY/10-M07

DEPARTMENT OF THE AIR FORCE

AIR UNIVERSITY

AIR FORCE INSTITUTE OF TECHNOLOGY

Wright-Patterson Air Force Base, Ohio

AFIT/GA/ENY/10-M07

INVESTIGATION OF A NOVEL COMPACT VIBRATION ISOLATION SYSTEM FOR SPACE APPLICATIONS

THESIS

Presented to the Faculty of the
Department of Aeronautical and Astronautical Engineering
Graduate School of Engineering and Management
Air Force Institute of Technology
Air University
Air Education and Training Command
in Partial Fulfillment of the Requirements for the
Degree of Master of Science in Astronautical Engineering

Steven D. Miller, B.S.
Second Lieutenant, USAF

March, 2010

AFIT/GA/ENY/10-M07

INVESTIGATION OF A NOVEL COMPACT VIBRATION ISOLATION SYSTEM FOR SPACE APPLICATIONS

Steven D. Miller, B.S.
Second Lieutenant, USAF

Approved:

Lt Col Eric D. Swenson (Chairman)	Date
Dr. Richard G. Cobb (Member)	Date
Lt Col Carl R. Hartsfield (Member)	Date
Dr. Jonathan T. Black (Member)	Date

AFIT/GA/ENY/10-M07

Abstract

A novel compact vibration isolation system was designed, built, and tested for the Space Chromotomography Experiment (CTEx) being built by Air Force Institute of Technology (AFIT) researchers. CTEx is a multifunctional experimental imaging chromotomographic spectrometer designed for flight on the International Space Station (ISS) and is sensitive to jitter caused by vibrations both through the support structure as well as those produced on the optical platform by rotating optical components. CTEx demands a compact and lightweight means of vibration isolation and suppression from the ISS structure. Vibration tests conducted on an initial isolator design resulted in changes in the chosen spring and damping material properties but confirmed finite element (FE) model results and showed that the spring geometry meets preliminary design goals. The FE model served as a key tool in evaluating material and spring designs and development of the final drawing sets for fabrication. Research efforts led to a final design which was tested in the final flight configuration. This final configuration proved the potential for a compact means of vibration isolation for space applications.

Table of Contents

Page

Abstract iii

List of Figures vii

1. Introduction 1

2. Background 4

2.1 Chromotomographic Experimental Imager (CTEx) . . 4

2.2 International Space Station Environment 5

2.3 Existing Space Vibration Isolation Methods 8

2.3.1 Finite Element Modeling 10

2.3.2 Dynamic Characterization 11

3. Experimental Design and Setup 13

3.1 Concept 13

3.2 Modeling and Design 14

3.2.1 CAD Solid Model 14

3.2.2 Desktop Concept 15

3.2.3 Finite Element (FE) Modeling 16

3.3 Isolator Prototype 19

3.3.1 Stainless Steel Springs 19

3.3.2 Aluminum Springs 19

3.3.3 Viscoelastic Damping 20

3.4 Mock Optics Platform Assembly 21

3.4.1 Breadboard 21

3.4.2 Isolators and I-Beams 21

Page

3.5 Static Loads 23
3.6 Laser Vibrometer Characterization 24
3.7 Vibration Exciter Characterization 25

4. Results and Analysis 28
4.1 CAD and FE Model 28
4.2 Stainless Steel Springs 29
4.2.1 Static Load Testing 30
4.2.2 Dynamic Testing 32
4.3 Aluminum Springs 35
4.3.1 FE Model Extrapolation 35
4.3.2 Static Load Testing 35
4.3.3 Dynamic Testing 37
4.4 Damping Effects 39
4.5 Mock Optics Platform Assembly 41
4.5.1 Sine Sweep Characterization 41
4.5.2 Breadboard Damping Effects 43
4.5.3 Random Vibration 44

5. Conclusions 46
5.1 Overall Design and Test 46
5.2 Damping Considerations 47
5.3 Space Application 48
5.4 Future Work 49

Appendix A. MATLAB Analysis Code 51
A.1 Laser Vibrometer Data Analysis 51
A.2 Vibration Exciter Data Analysis 53

Page

Appendix B. Fabrication Drawing Sets 62

Bibliography 71

List of Figures

Figure		Page
1	JEM-EF typical payload envelope adapted from "Kibo Handbook" [8:p 4-18]	2
2	Hexapod vibration isolation arrangement	3
3	Photo of CTEx ground based prototype [7]	5
4	Japanese module "Kibo" of the International Space Station [1]	6
5	Vibration accelerations imposed on an experimental payload at point of attachment to the JEM-EF [11:§2.1.5]	7
6	JEM-EF vibration acceleration disturbance limitations for an experimental payload [11:§2.1.5]	7
7	Six-strut linear isolator arrangement known as the UltraQuiet Platform [3]	8
8	One of three bi-pod and shock tower constituents of the VISS [5]	9
9	Original design concept	13
10	First isolator prototype design	15
11	Conceptual model	16
12	First isolator prototype FE model	17
13	Changes in spring design from FE analysis	17
14	CAD model showing the final isolator prototype design	18
15	Photograph of the isolator prototype	19
16	Isolator prototype with damping applied	21
17	Mock breadboard construction	22
18	Shaker head with I-beam support structure	23
19	Static load test setup	24
20	Laser vibrometer setup	25
21	Single isolator on vibration exciter with 30 pound mass attached to the jewel	26

Figure		Page
22	Mock optics platform and isolator assembly on vibration exciter	27
23	FE model final spring shape analysis with applied static loads	28
24	FE model predicted displacements from vertical 40 lb load with stainless steel springs: jewel displacement = 0.0125 in	29
25	FE model predicted displacements from vertical 100 lb load with stainless steel springs: jewel displacement = 0.0313 in	30
26	Vertical load test results for stainless steel springs with linear regression	31
27	Lateral load test for stainless steel springs with linear regression	31
28	Opposing lateral load test for stainless steel springs with linear regression	31
29	FE model vibration modes of isolator with stainless steel springs with additional 10 lb mass	33
30	Damping effect with no additional mass and stainless steel springs	35
31	Vertical load test for aluminum springs with linear regression	36
32	Lateral load test for aluminum springs with linear regression	36
33	Opposing lateral load test for aluminum springs with linear regression	37
34	Single isolator with no additional mass attached	38
35	Vibration exciter sine sweep of single isolator with 30 lbs additional mass attached	40
36	Lateral sine sweep of a single isolator attached to the breadboard assembly	42
37	Longitudinal sine sweep of a single isolator attached to the breadboard assembly	42
38	Vertical sine sweep of a single isolator attached to the breadboard assembly	43
39	Vertical random vibration of a single isolator attached to the breadboard assembly	45

INVESTIGATION OF A NOVEL COMPACT VIBRATION ISOLATION SYSTEM FOR SPACE APPLICATIONS

1. Introduction

A vibration isolation system must be developed for the Air Force Institute of Technology's (AFIT) Space Chromotomography Experiment (CTEx). In short, the CTEx instrument is a highly sophisticated imager that is sensitive to vibration. The concept utilizes a spinning prism to optically disperse the light prior to reaching the sensor where the image is stored along with the time of recording and angle of the prism. The spatial spread of the light passing through the prism makes it possible to rapidly decompose the image in order to determine its spectral content. The goal of the experiment is to characterize both the spectral, spatial and temporal aspects of fast transient combustion events using chromotomography. The CTEx imager is being designed to attach to the International Space Station (ISS) as a proof of concept experiment.

CTEx is composed of a front end optical telescope with slow and fast steering mirrors for tracking and small vibration corrections, respectively. Behind the telescope is a double prism which is housed in a rotating body placed directly in front of the high speed camera. The design is sensitive to vibrations both during launch and while attached to the ISS. CTEx is proposed to be attached to the Japanese Experimental Module (JEM) - Exposed Facility (EF), named "Kibo", of the ISS. The physical dimensions of the maximum payload envelope prescribed for the JEM-EF, depicted in Fig. 1, require precise planning and utilization of all available space. A unique vibration isolation system is required to meet the vibration and spatial demands of the CTEx instrument while attached to the JEM-EF.

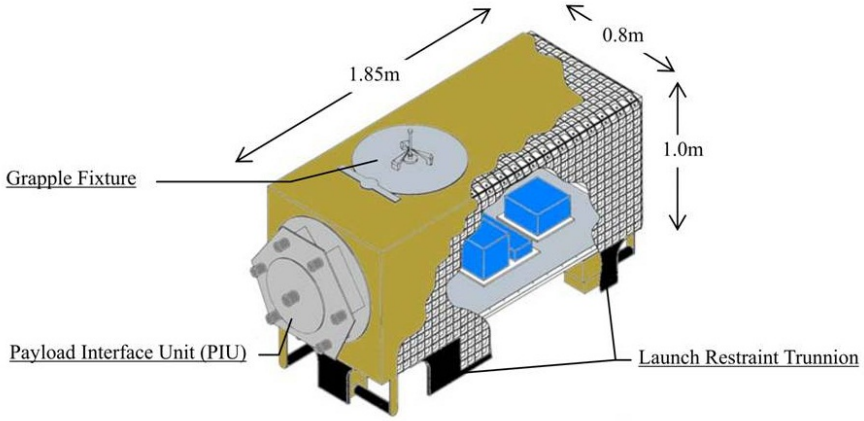

Figure 1 JEM-EF typical payload envelope adapted from "Kibo Handbook" [8:p 4-18]

Typical vibration isolators are designed specifically to address linear motion in terms of isolation and vibration energy suppression. If only one translational axis of motion is of concern then this type of simple isolator, like the shock absorbers on an automobile, is ideal. However, rarely is this the case. If the application does not have translational or rotational constraints, simple isolators will not work. Many applications require that a certain platform or object be isolated from vibration in any direction implying an arrangement capable of isolating three axis translation and rotation.

In optics applications, the design process begins with an optics platform that is extremely stiff. In other words, the platform on which the optics are physically mounted is fabricated to act as much as possible like a rigid body but with very high natural frequencies. A rigid body is ideal for optics as it implies that no point moves with respect to any other point keeping the optical elements in alignment. This optic platform is then attached to the surrounding support structure with an appropriate isolation system which minimizes vibrations from the surrounding structure leaving a stable and relatively low vibration environment for the optics.

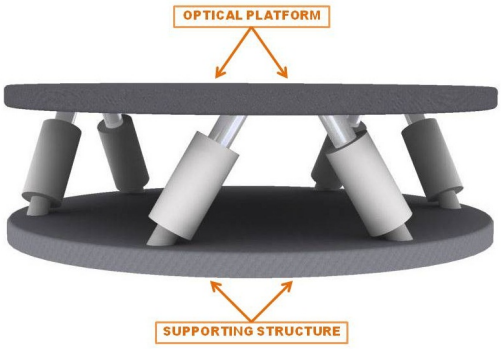

Figure 2 Hexapod vibration isolation arrangement

As previously mentioned, most isolation assemblies are designed to work only for linear motion. If a rigid body assumption of the optics platform is made, a hexapod arrangement of linear isolators is acceptable to isolate the requisite six degrees of freedom (DOF) (three orthogonal rotations and three orthogonal translations). Figure 2 shows a standard arrangement of linear isolators or actuators that provide for six DOF of a single rigid body attached to the top. In reality, even a very stiff optical platform will have natural vibration modes that will be excited depending on frequency content of the excitation source. In a perfectly ideal, but unrealistic situation, the optics platform would be isolated from the superstructure by connecting it with isolators that are not able to transmit motion in all six degrees of freedom at *every* attachment point. This concept began the idea of the compact triple isolator assembly.

2. Background

2.1 Chromotomographic Experimental Imager (CTEx)

Researchers from the Air Force Institute of Technology are working on a novel hyperspectral chromotomographic imager designed to capture fast transient combustion events not possible with other hyperspectral imaging (HSI) techniques. This concept, known as the Space Chromotomography Experiment (CTEx), is designed to be employed from space in order to capture and characterize highly transient battlefield combustion events [4]. A ground based prototype instrument has been produced for testing and is shown in Fig. 3. A hyperspectral data cube contains two spatial dimensions (usually x and y) and a third spectral dimension. Other HSI methods record this information from a static scene over a long time period of tens of seconds to days by scanning across the 2D area to be imaged and sampling the spectral composition at each point. Rapid acquisition of hyperspectral data is currently limited to a point source. The CTEx imager seeks to break this boundary by rapidly characterizing a dynamic scene using a direct vision prism. In short, a rotating prism lies in front of the focal plane array (FPA), dispersing the visible light across the FPA. As the prism is quickly rotated, each successive image is captured along with the prism's angular position. This information is then processed using a technique known as chromotomography to reconstruct the image and produce a 3D hyperspectral data cube. Using a rapidly spinning prism and high speed FPA, a hyperspectral data cube can be captured in short enough time to characterize fast transients such as combustion events from explosive devices.

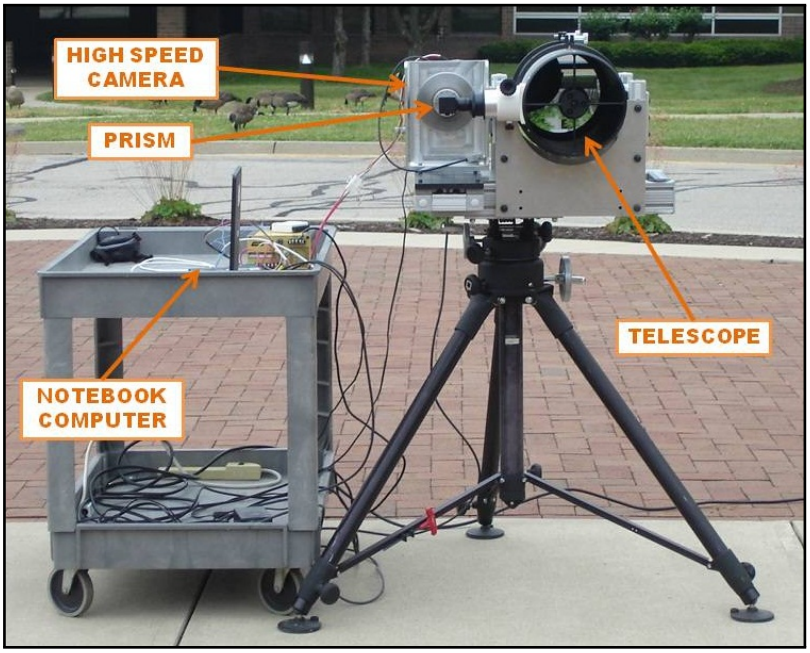

Figure 3 Photo of CTEx ground based prototype [7]

2.2 International Space Station Environment

Design of the International Space Station (ISS) began in 1982 with construction beginning in 1998 [8]. This manned facility orbits Earth at an altitude of approximately 400km once every 90 minutes. Japan, one of 15 countries involved in the project, has created an experimental facility on board the ISS named Kibo. The Japanese Experimental Module (JEM), as it is more formally known, consists of a pressurized module as well as an External Facility (EF). The JEM-EF is the intended location for the CTEx instrument. Transport to the JEM-EF involves a launch and ride to orbit on the autonomous, unmanned H-IIB transfer vehicle (HTV). After capture by the ISS remote manipulator arm, the HTV is attached to the station. A specialized pallet containing up to three experimental payloads destined to the JEM-EF is removed from the HTV and placed on Kibo's external facility. Using Kibo's own remote manipulator system, each experiment is removed from the pallet and attached to the EF's equipment exchange unit which, among other things, supplies the experiment with power and ground communications.

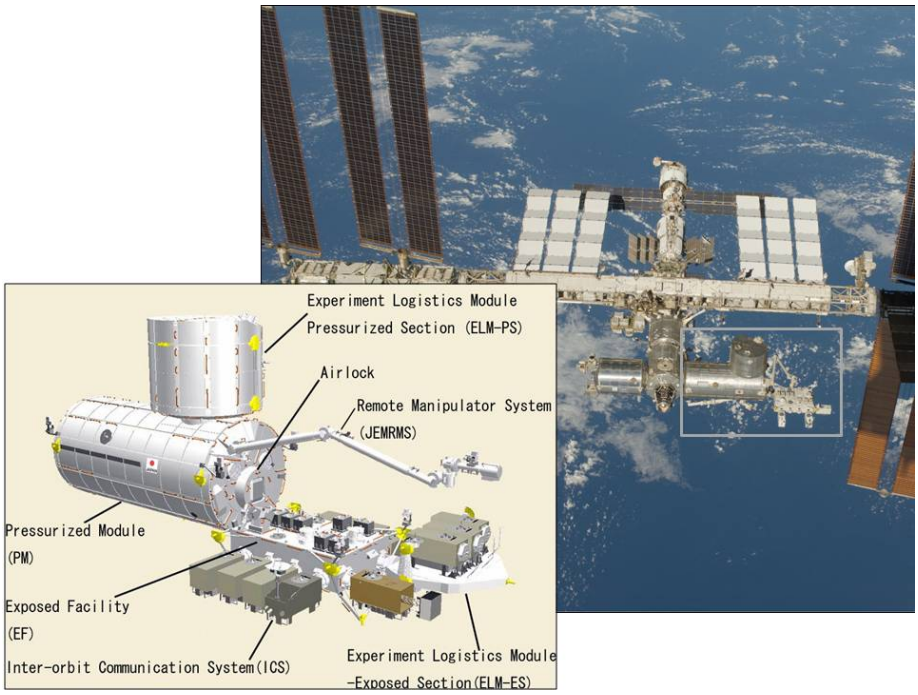

Figure 4　Japanese module "Kibo" of the International Space Station [1]

From the JEM-EF, the CTEx instrument will have a relatively stable platform form which operational tests will be conducted. The EF is designed as a microgravity research environment with minute vibration levels [11]. Figure 5 shows the expected accelerations imposed on an experimental payload at the payload interface unit (PIU) where the experiment attaches to the EF. There also exists a constraint that the experimental payloads may not impose vibration accelerations greater than depicted in Fig. 6 to the EF. Though the vibration environment on the ISS is relatively small for most applications, the CTEx instrument is highly sensitive to any jitter causing vibration and makes this a unique case where even low levels of mechanical noise must be removed.

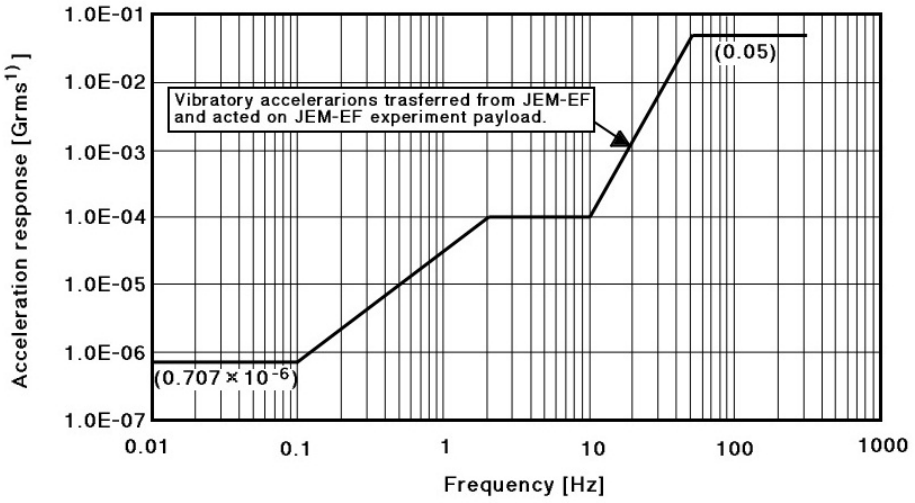

Note (1) Grms: RMS acceleration in 1/3 octoave bands averaged over 100 sec.
Note (2) The above is vibratory accelerations transferred from JEM-EF and acted on JEM-EF experiment payload in all the states including dynamic and trasient phase.
Note (3) The above is specified at the EFU/PIU interface.

Figure 5 Vibration accelerations imposed on an experimental payload at point of attachment to the JEM-EF [11:§2.1.5]

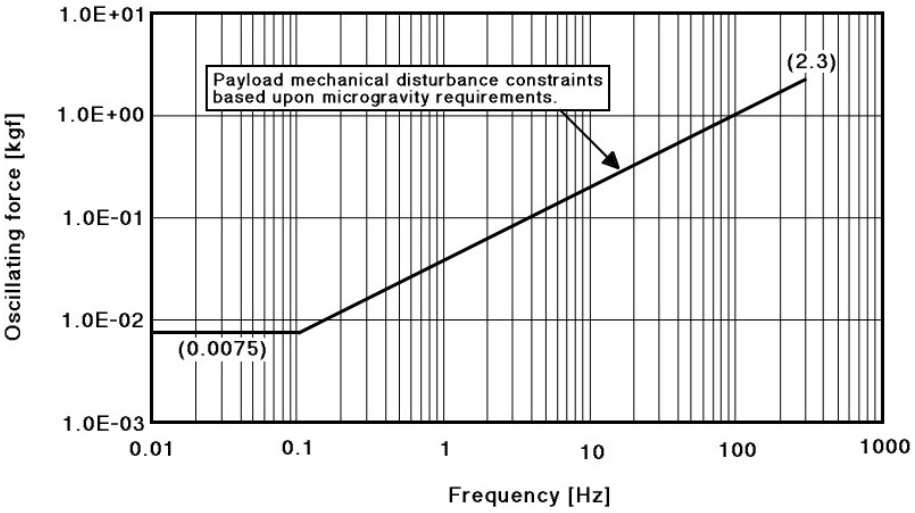

Note (1) The above shall be satisfied in all the states including the dynamic/transient phase.
Note (2) The above is defined at the EFU/PIU interface.

Figure 6 JEM-EF vibration acceleration disturbance limitations for an experimental payload [11:§2.1.5]

2.3 Existing Space Vibration Isolation Methods

Vibration isolation is not a new concept for space applications with low tolerances to jitter and high demands for stable and reliable platforms. Two environments exist within the broader category of space vibration: space launch, and on-orbit operations. One such isolation system for launch applications is known as SoftRide and has been implemented on numerous space and missile launches [9]. The "SoftRide MultiFlex Isolation System" is a CSA patented design for multidirectional loading but primarily attenuates axial launch loads. The purpose of the vibration isolation system for the CTEx imager is intended for space on-orbit operations, however, the the simplicity of the SoftRide spring geometry and damping technique is applied in the CTEx isolator assembly.

On-orbit isolation is most often performed with several linear vibration isolators arranged in various configurations to meet the requirements of the particular payload. One such system is the UltraQuiet platform which utilizes the typical six-strut isolation mount as well as both passive and active isolation techniques [3]. This large system of linear isolators is shown in Fig. 7.

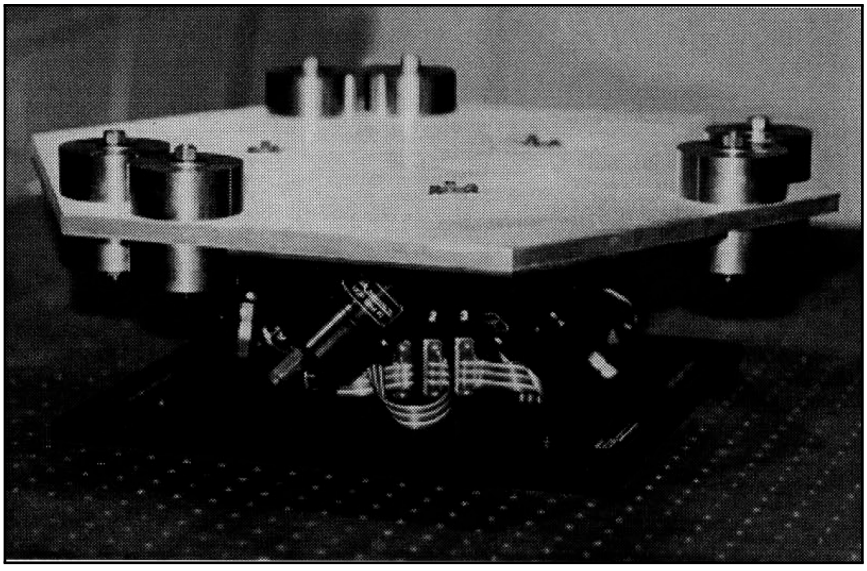

Figure 7 Six-strut linear isolator arrangement known as the UltraQuiet Platform [3]

Other systems, like the "Vibration Isolation and Suppression System" (VISS) [5] use bi-pod linear actuators located at several attachment points on an optical platform to achieve results similar to the six-strut configuration. The VISS, shown in Fig. 8, is similar to CSA Engineering's Satellite Ultraquiet Isolation Technology Experiment (SUITE) but further provides steering control. The CTEx removes the steering requirement from the vibration system and transfers it instead to the optical elements. Each of these types of isolators require detailed knowledge of the optical system and vibration environment to employ a complex means of sensors and control algorithms, actively controlling the actuators that provide the desired stiffness and damping to the system [12].

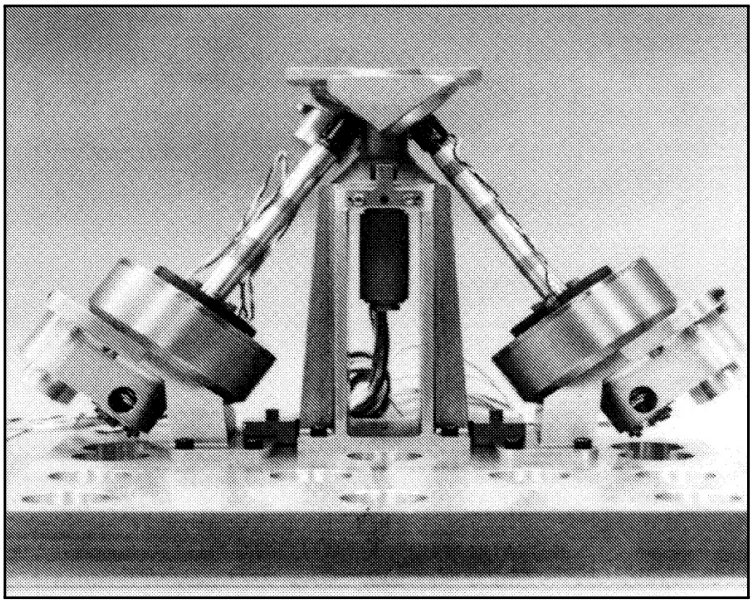

Figure 8 One of three bi-pod and shock tower constituents of the VISS [5]

The CTEx isolation system seeks to provide similar vibration isolation as the aforementioned systems and techniques but with a much simpler and compact design. The CTEx isolator must provide multidirectional compliance as with the VISS, SUITE and UltraQuiet designs though is limited by physical space requirements to be more compact in design than a typical hexapod-supported platform. This new isolator design works with the simplicity of the SoftRide spring geometry in a new

and unique arrangement to act as these traditional systems, but within a significantly smaller space requirement and without active control techniques.

2.3.1 Finite Element Modeling. Finite element (FE) modeling and analysis is a method by which field quantities, described by differential equations, are numerically iterated through a system to arrive at a solution from a set of known initial conditions [6]. FE analysis can be completed for field quantities such as heat, stress, displacements, and electric/magnetic fields. This method is applied to vibration isolation problems by first modeling the physical assembly then computing the stress and strain at nodes that define the problem. Each physical component is modeled by first creating or importing the appropriate geometry, usually from a CAD software package, and then meshing. The mesh is a placement of known elements that represent the geometry and each can be mathematically described with algebraic equations. Within each element of the mesh, several nodes are created at points where information about the field quantity (stress, strain, etc.) is desired. Known boundary conditions such as physical constraints are applied to the model as well as known inputs such as forces. The model is analyzed by solving for desired values at each node and then displaying these using color contours and/or showing physical displacements.

An FEA software package is typically used for all functions of preprocessing, numerical analysis (solving), and finally postprocessing. Preprocessing involves the application of small discrete elements to the model geometry known as meshing. This is a critical phase where mesh size and element types are carefully chosen usually from experience or by short trial and error to accurately describe the physical model. It is in this phase that the various parts are connected by inserting constraints to the field properties at particular nodes. The numerical analysis is accomplished separately by describing the entire problem mathematically in matrix form and solving for the unknown quantities at the nodes of the mesh. Interpolation functions are used to realize values within each element. Solvers can be used for both linear and non-linear

systems. The results of the solver are then graphically displayed in postprocessing. For analysis of physical field properties, stresses are usually displayed as varying color contours along with a predicted deformation of the assembly.

Results of FEA are used to update the physical design. At some point, FE predictions are compared to experimental results in order to tune the model. This tuning is done to revise the model such that it accurately represents the actual measured field quantities. Once a model is tuned, further development changes or modifications can be made with higher levels of confidence. FE modeling can significantly reduce the number of costly physical models produced for experimental testing before arriving at a final design. Further, the final design can then be used to tune the FE model once again to predict the behavior of the assembly in various applications.

2.3.2 Dynamic Characterization. Dynamic testing or characterization is utilized to understand the behavior of a system by studying the input excitation to output response relationship [2]. In the case of an isolation assembly, the transmissibility of the device is of primary concern. This is accomplished by analyzing the frequency response function (FRF) for the system commonly referred to as a transfer function in a control system environment. FRFs are complex in nature and relate both the magnitude and phase associated with the response. For the purposes of vibration isolation, the magnitude is of much greater importance than is the phase. The FRF is a relationship, not an absolute. It displays the output of a system with respect to a given unit input varied throughout the frequency domain in question. In practice, an input or excitation is established and measured along with the measured output. The output is then simply divided at each frequency by the respective input to obtain the magnitude of the FRF. Because this is a standard output-to-input ratio with a large range of values, the magnitude is usually expressed in Decibels.

In terms of vibration isolation systems, the most important characteristic must describe how well the device isolates, or inversely, how transmissive the device is. It is impossible to arrest all vibration transmission through a physical device. If nothing else, a free body mode will exist where the device tracks the motion of the support structure. The remaining degrees of freedom will each have a natural resonance at somewhat higher frequencies. The goal then in isolator design is to reduce the peak's magnitude and to move the natural frequencies of the system as low as possible, or in other words, closer to the free body mode to take advantage of the 'rolloff' of the FRF past the resonance.

Application of this concept of low frequency compliance works well with the CTEx optical system containing both a slow steering objective mirror and a fast steering image stabilization mirror. The slow steering mirror accounts for the free body mode of the space station in order to track the ground objective while moving across Earth's surface. An appropriate vibration isolation system combined with the space station and CTEx instrument must only be transmissive to those frequencies that can be tolerated optically through the use of the fast steering mirror. Accordingly, the natural frequencies apparent in the FRF must be low enough that they do not exceed the capability of the actively controlled optics and that all other frequencies be substantially attenuated.

3. Experimental Design and Setup

3.1 Concept

In short, a hexapod-like assembly could be designed with six linear isolators, as shown in Fig. 2, and made to attach at each point on the optical platform. Simply modifying existing hexapod designs would result in a complex and potentially very large attachment structure as the hardware size required to support six individual attachments would make this concept impractical for the CTEx application. The goal is to create a less complex isolator that is compact enough to place at each desired attachment point on the platform but allow for isolation and suppression of motion in more than one direction. The first cut attempt at this goal is shown in Fig. 9 in which three individual 'C'-shaped springs are arranged on pedestals each 120° apart in a circular pattern. Also shown are rubber dampers attached near the elbow of the springs with thin sheet metal plates to provide a constraining layer.

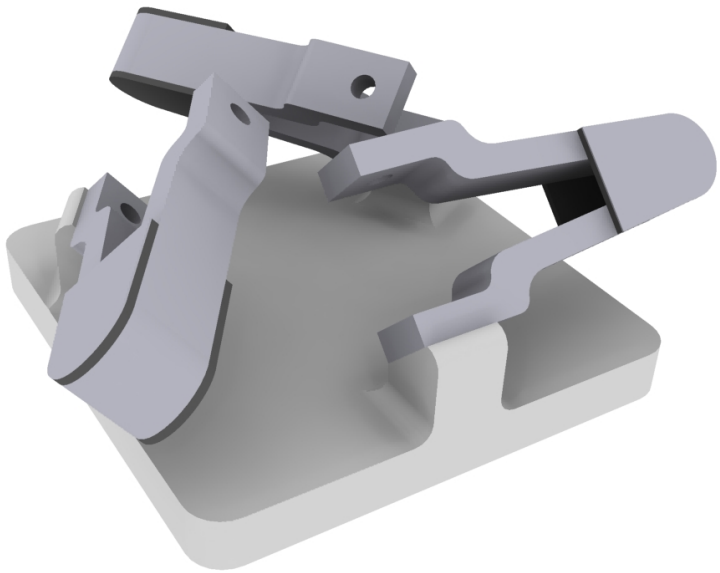

Figure 9 Original design concept

The motivating idea behind this particular design is to take geometrically simple springs and arrange them in such a way as to provide relatively similar characteristics in stiffness and later damping to translation in any three dimensional direction. The geometry also allows for small rotations as well, though this being a much stiffer motion. The most difficult element of this design is to create the common point to which the three springs and the optical platform would attach. Several concepts involving both rigid elements and rotational joints were examined.

3.2 Modeling and Design

3.2.1 CAD Solid Model. The unique geometric arrangement of the isolator design meant that 3D CAD visualization and prototyping software was the answer to beginning the modeling and analysis of various arrangements and iterations on the design. This process began by designing a base plate and pillar assembly that was easily fabricated and then modifying the initial spring shape to the simplest form. A thin spring with a constant cross section and with only one bend and two attachment points was created. This left only the design of the central attachment point. After much discussion and exploration of the trade space involving both a rigid and rotational joint as well as their resulting effects on the isolation and suppression of the optical platform of the CTEx instrument, it was decided that a simple rigid center piece would properly complete the design. Using the 3D CAD software, a relatively complex shape was constructed to accept threaded attachments for each of the springs and a larger, single attachment point for the optical platform. This initial design assembly is shown in Fig. 10. Due to its appearance, this central attachment device was nicknamed the 'jewel' and will subsequently be referred to as such.

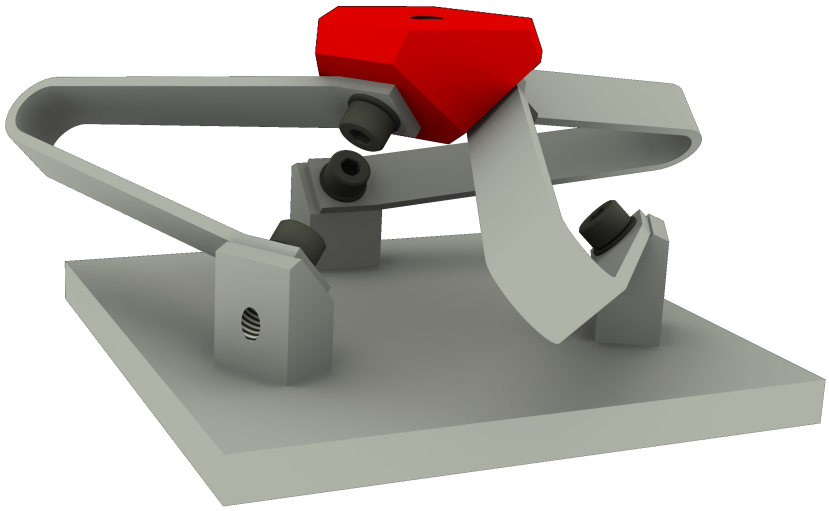

Figure 10 First isolator prototype design

3.2.2 Desktop Concept. After finishing the initial design, it was appropriate to create a physical model of the isolator in order to better understand what characteristics this device may have after complete fabrication. A simple base plate and pillar system was constructed by hand from oak with the springs being simulated with bent aluminum sheet metal. The jewel, with its complex shape, was printed on a 3D rapid prototyping machine. The entire assembly is shown in Fig. 11.

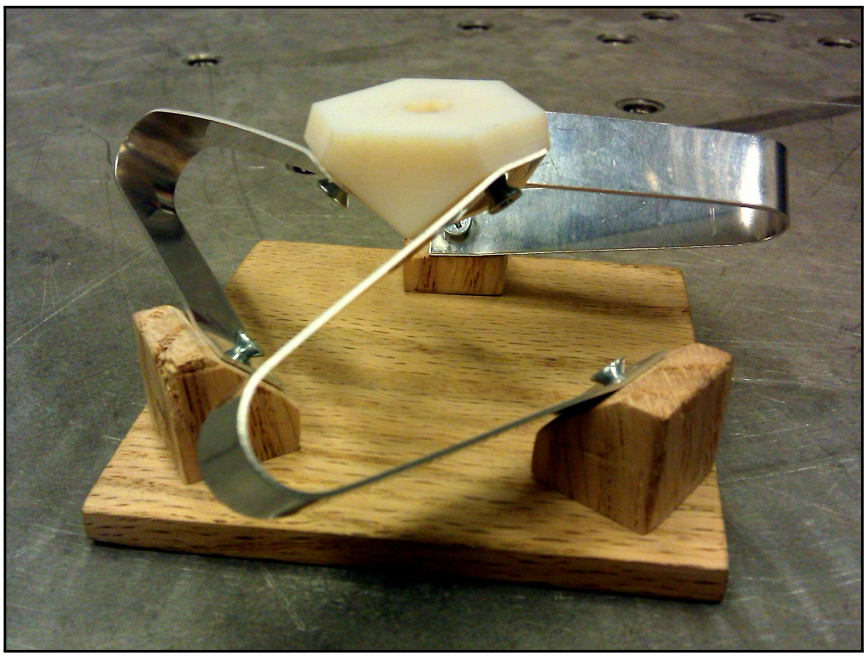

Figure 11 Conceptual model

3.2.3 Finite Element (FE) Modeling. The solid CAD model was imported into a FE modeling and analysis software package in order to evaluate the latest design iteration and make modifications as necessary to meet design goals as shown in Fig. 12. Not surprisingly, the simple uniform shape used for the springs was not ideal and showed areas of high stress concentrations. Using the output from the finite element analysis (FEA) showing stress concentration, the 3D CAD model was updated to reduce high stress levels by specifying a greater thickness in high stress areas and subsequently thinning other areas with low stress values. The model was again imported and FE analysis completed, a process that was completed two more times to arrive at the final design. Figure 13 compares the initial and final designs.

The spring design as shown in Fig. 13(b) has a variable cross section and thus the stress is more uniformly distributed. The width of the spring was kept constant in order to simplify the fabrication process. This geometry resulted in a very uniform stress fields throughout the spring as seen in both the static and dynamic response. This spring design can easily be cut from metal plate stock using either a water jet

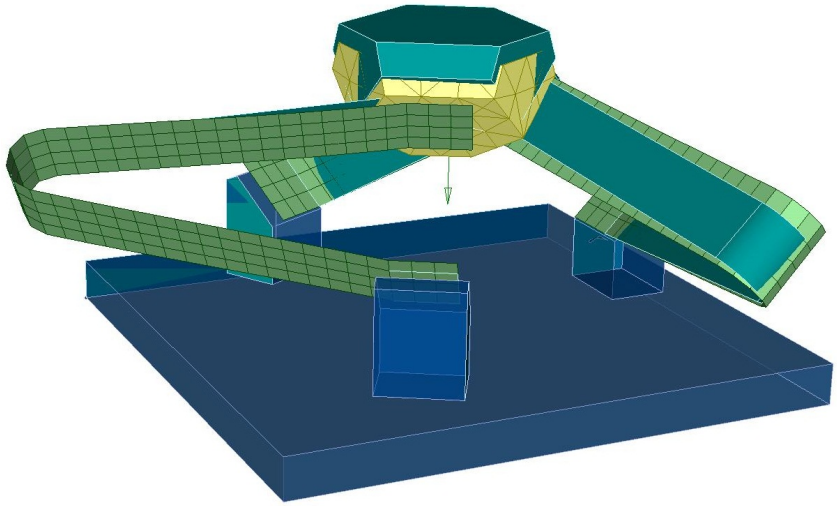

Figure 12 First isolator prototype FE model

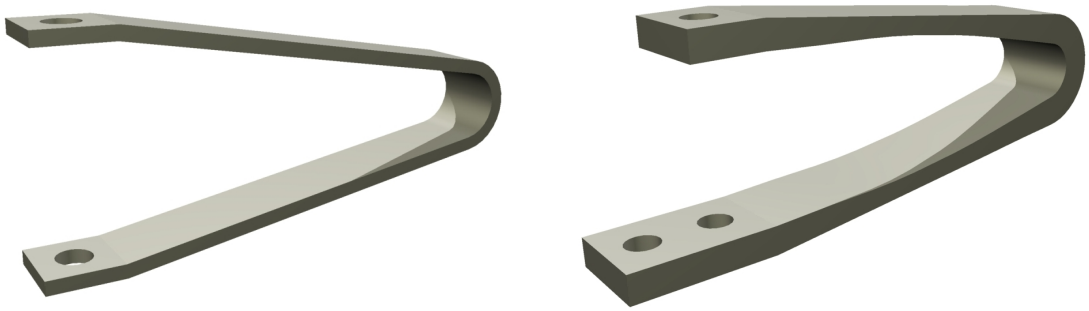

(a) Original simple bent steel spring.

(b) Revised spring with variable cross section.

Figure 13 Changes in spring design from FE analysis

cutting machine or more precisely with electrical discharge machining. In addition, an extra hole was added at the base attachment point of the spring in order to keep the spring from rotating in the assembly as evidenced by the FE model.

Only a few more design specifications had to be chosen before the assembly's fabrication drawing set could be sent to the fabrication facility. First was a choice in materials. Since this was to be a first cut prototype and used only for testing and characterization of the design, inexpensive mild steel was chosen for all elements except the springs. Being very compact, less than two inches in height, with very small springs and a known static load of at least 50 lbs, the spring material was initially chosen to be a stiff and durable 316 alloy stainless steel. The base plate was modified to attach either to an isolated lab bench or vibration exciter and a large hole cut in the center to provide access for static load testing. The jewel and pillars were also modified slightly to allow for simpler and more timely fabrication. The final CAD model is shown in Fig. 14.

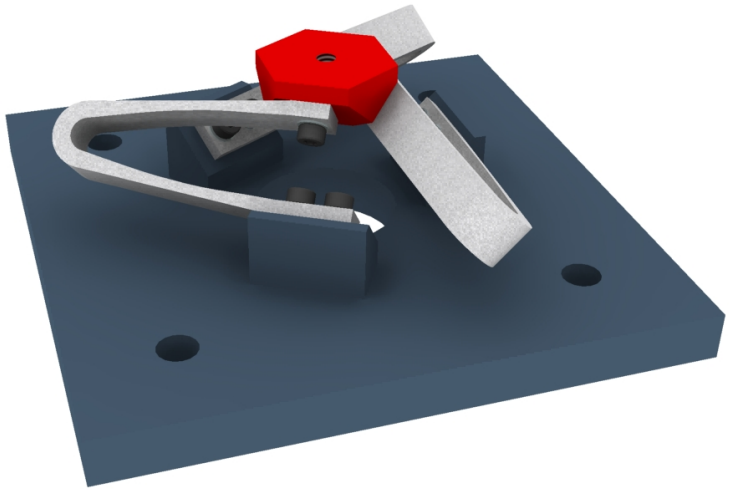

Figure 14 CAD model showing the final isolator prototype design

3.3 Isolator Prototype

3.3.1 Stainless Steel Springs. As previously mentioned, the springs were originally 316 alloy stainless steel and were not heat treated as would normally be done for spring applications. The heat treating process would increase the material's yield stress for applications with repeated high stresses making the untreated 316 stainless selected a poor candidate. The heat treatment process is not necessary this early in the design phase because test loads and number of cycles are minimal. Figure 15 shows the completed prototype utilizing the stainless steel springs. The base plate and pillars are painted blue as were shown in the CAD model, see Fig. 14, and the jewel attachment point shown in red for clarity.

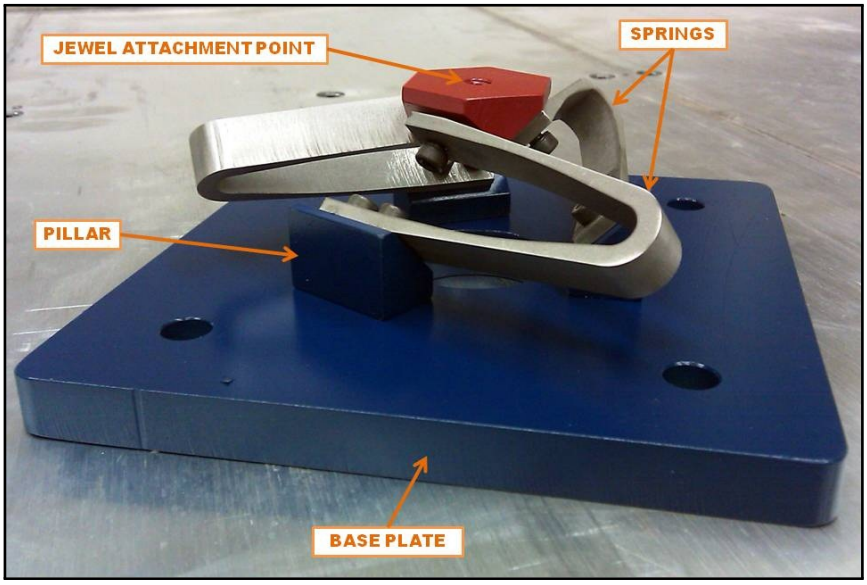

Figure 15 Photograph of the isolator prototype

3.3.2 Aluminum Springs. Several sets of 6061-T6 alloy aluminum springs were made. The aluminum selected has great general purpose machining qualities as well as good heat treatment giving it a higher than normal yield stress value. These sets were made to provide a more compliant spring as compared to the 316 stainless used in the initial prototype. Though aluminum is not generally considered a spring material, within the small displacements and low cycles expected in testing, it was

considered acceptable to accurately test shape, geometry, and stiffness properties. These aluminum springs will also be used in the following isolator assemblies used to test a mock optics platform.

3.3.3 Viscoelastic Damping. Working with such a unique geometry it was difficult, even with the FE model, to predict the best location to apply viscoelastic damping. Based on the thin cross section of the springs it was plausible that much of the motion of the jewel would result in an opening or closing motion of at least one of the three springs. This being the assumption, rubber dampers were created and applied to the outsides of the springs using Scotch Grip 1300L neoprene contact adhesive. A constraining layer of aluminum sheet metal was cut to the same shape and adhered in turn to the outside of the rubber dampers. In order to ensure maximum available damping and repeatability, machine screws were added to act as through bolts slightly compressing the rubber against the springs.

Initial tests were conducted with soft rubber material available at the time was butyl rubber from an aircraft inner tube. Because the inner tubes had to be cut by hand, sheets of rubber were purchased to take their place. Two types of rubber were purchased to experiment with differences in hardness and elongation specifications. These were buna-N and neoprene, both have high elongation properties but different hardness ratings with the neoprene being the softer of the two materials. These rubber sheets, along with the constraining aluminum sheet metal layers, can easily be cut to the exact spring shape with the water jet cutting machine used to produce the steel and aluminum springs. The isolator prototype is again shown in Fig. 16 with the butyl hand cut inner tube rubber dampers applied.

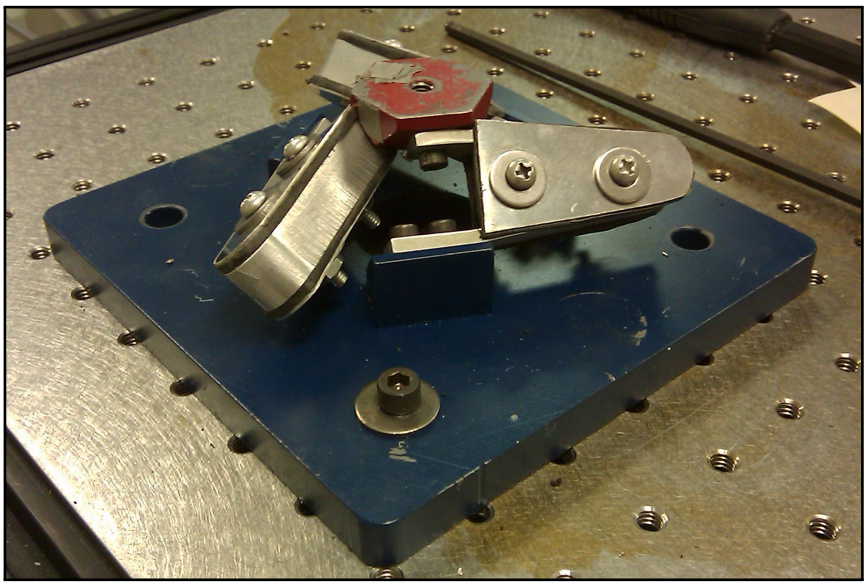

Figure 16 Isolator prototype with damping applied

3.4 Mock Optics Platform Assembly

3.4.1 Breadboard. In order to test the isolator assembly for use with the CTEx optical platform along with the front end optics, a mock optics platform was produced. The mock platform or breadboard had to be very stiff in order to mimic the CTEx breadboard. The breadboard must also represent the nominal weight of the optics platform with appropriate components. In order to accomplish this quickly and with little manufacturing expense, a breadboard design was completed with 1/4 inch thick 6061-T6 aluminum plates placed on either side of an internal structure. The internal framing was created from 80/20 Inc.'s one inch square t-slot extruded aluminum stock and assembly hardware. Shown in Figure 17 is the CAD design of the internal structure as well as photos of the actual assembly. With the aluminum plates bolted in place through the internal frame a stiff platform was created with similar dimensions to the actual CTEx flight hardware and weighing in at approximately 97 lbs.

3.4.2 Isolators and I-Beams. While the mock optics platform was in the fabrication process, three more isolator assemblies were manufactured with slight

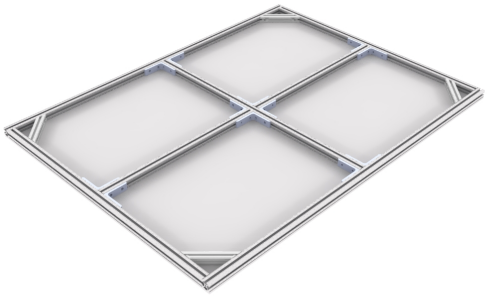

(a) CAD Design with top plates removed

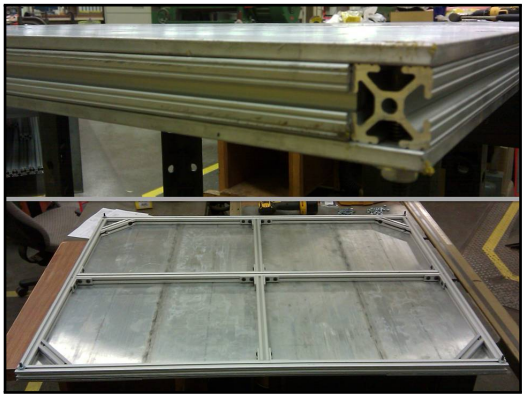

(b) Breadboard with edge close up and internal view

Figure 17 Mock breadboard construction

modifications to their base plates for attachment purposes. These isolators were made to attach to the optical platform at the jewel and to the superstructure of the CTEx payload assembly on the ISS. In order to accurately test this setup, the AFIT vibration exciter shaker head interface had to be modified to support the isolators under the breadboard at appropriate locations. Special cleats were fabricated to attach aluminum I-beams to the shaker head which were in turn drilled and tapped to receive the base plates of the isolators. The I-beam layout on the shaker head is shown in Fig. 18. Each of the three isolators are attached near the ends of the beams and attached to the breadboard through bolts at three locations.

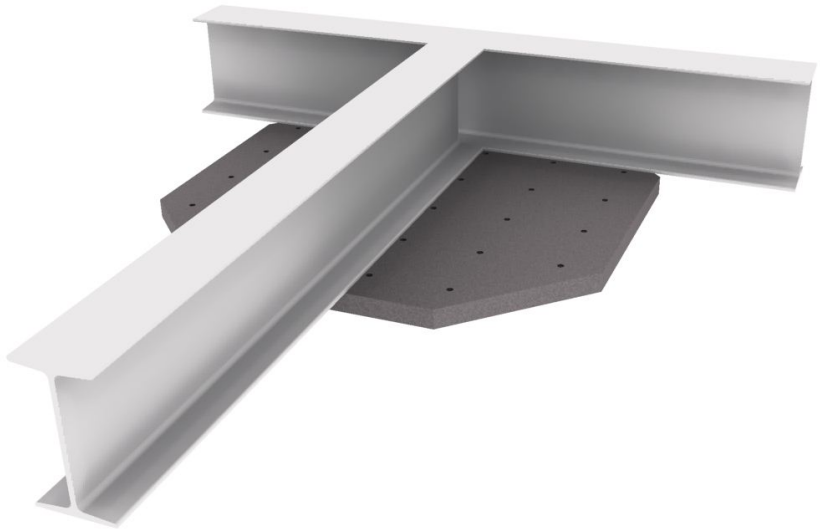

Figure 18 Shaker head with I-beam support structure

3.5 Static Loads

In order to accurately tune the FE model of the actual isolator prototype, both dynamic and static responses were collected. Figure 19 shows the test setup used to measure the jewel displacements relative to the base plate under known loads in particular directions.

Figure 19(a) shows the setup as used for vertical static load characterization. The isolator base plate was clamped to rigid support beams and an eye bolt threaded into the through hole extending from the bottom of the jewel. A depth micrometer was positioned to measure the relative displacement of the jewel with respect to the base plate. A rope was used to suspend weights from the isolator.

Similarly, Fig. 19(b) shows the test setup for lateral or side loads on the jewel. This setup holds the isolator base plate vertically and places the loads on the jewel minimizing moments. The arrangement was used twice: once in the configuration as shown, and once with the base plate rotated 180°. Essentially, pulling both up and

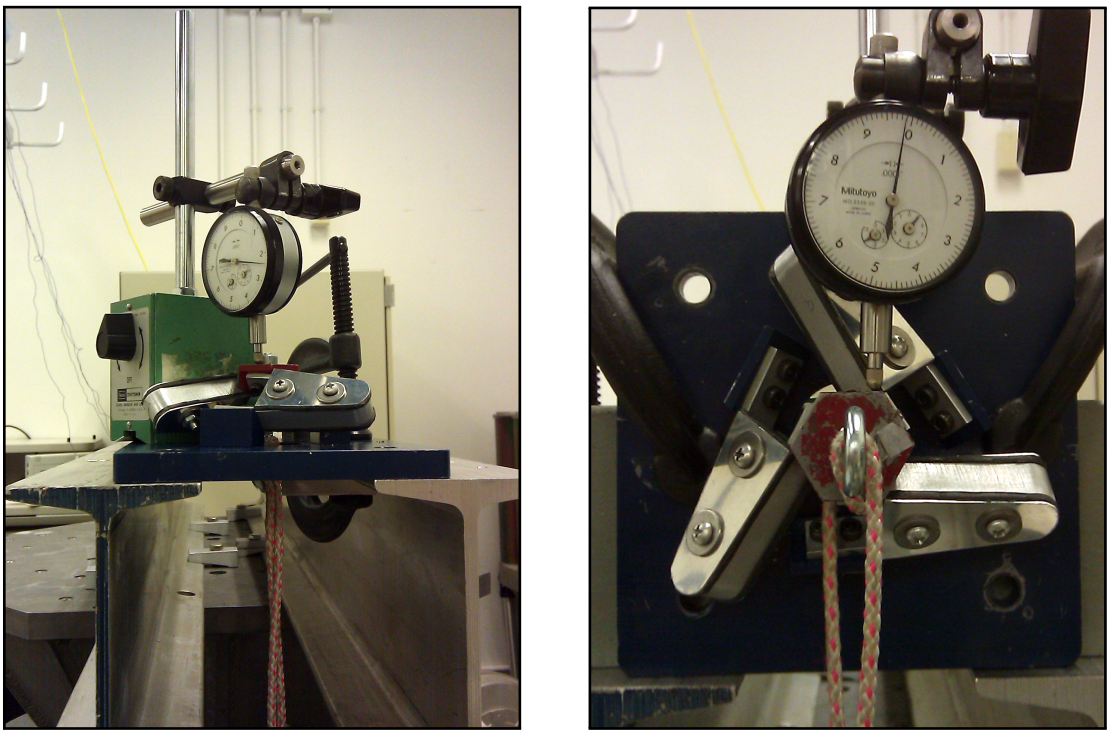

(a) Vertical load testing (b) Side load testing

Figure 19 Static load test setup

down on the jewel as shown. This was done to see if there was a particularly stiff direction when pulling either towards or away from one of the springs.

In order to minimize any effects of slipping between the rubber dampers and springs, each static load test was initialized with the maximum weight used for a particular test. Displacements were recorded and weights were systematically removed. Using this process, the error in the measurements was considerably reduced from starting at zero weight and increasing. Actual displacements were recorded manually from the micrometer.

3.6 Laser Vibrometer Characterization

A laser vibrometer was used to initially characterize the properties of the isolator assembly both with and without damping, as shown in Fig. 20. A secondary goal of these tests was to properly tune the FE model in such a way as to produce similar

results to the physical assembly. In this manner, further design changes could be made to the model with higher confidence that the actual test article changes would produce similar effects.

The isolator assembly as well as a single spring are attached to an optics bench that provides a rigid surface. A calibrated, instrumented ping hammer was used to excite the assembly by striking only the jewel while the laser vibrometer measured the resulting velocities. Frequency response functions (FRFs) are computed from the input-output velocity and force measurements. Collecting FRFs was repeated several times on various springs for fabrication quality assurance purposes. Further, the isolator was ping tested with various sized weights up to 50 lbs attached to the jewel.

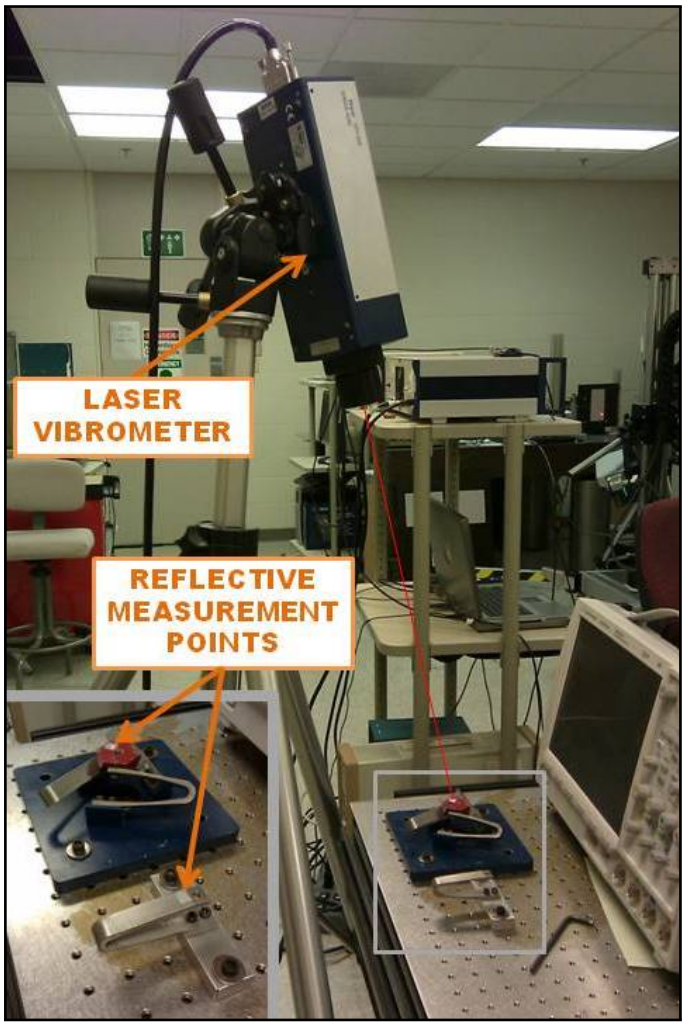

Figure 20 Laser vibrometer setup

3.7 Vibration Exciter Characterization

A large MB Dynamics C40HP vibration exciter or shaker was used to provide much greater input excitation levels than the ping hammer could and therefore

produce a more realistic input for larger accelerations. Unlike the ping hammer testing used to collect the impulse responses, the shaker was used either to sweep through the frequency range of interest with a sinusoidal signal or excite a wide range of frequencies with white noise at various excitation levels. The C40HP has a force rating of 5,000 lbs peak for sine inputs with a maximum acceleration of 100 g's and a two inch armature stroke [10].

This shaker device was used in a variety of different tests. First, the shaker was used in similar tests on the single isolator prototype with varying weights attached in the vertical direction, as shown in Fig. 21. Small accelerometers were used to measure the input and output responses, as shown in Fig. 21. Tests on the single isolator prototype were conducted again with and without damping in order to characterize the effects of this particular application of constrained layer damping.

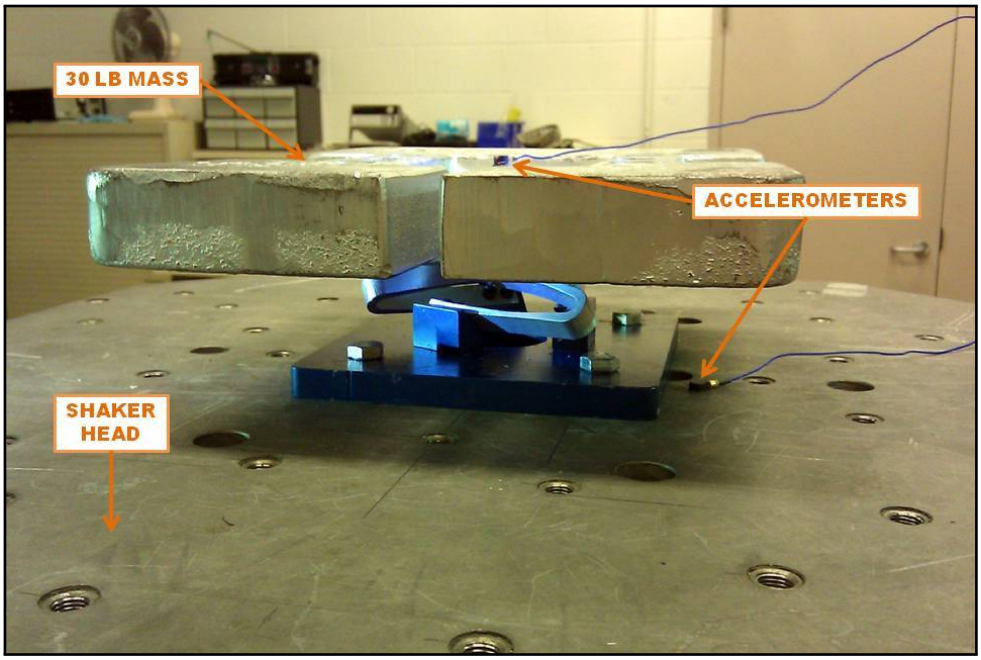

Figure 21 Single isolator on vibration exciter with 30 pound mass attached to the jewel

With the large I-beam attachment on top of the shaker head, as shown in Fig. 22, the entire breadboard and isolator assembly was tested. This setup, with an

additional 50 pound mass as shown, was used to test the response on the breadboard as well as the transmittance of the isolators in the vertical direction. The inset in the upper right corner shows a close up of the isolator attachment method from the I-beam to the optical platform. Reconfigured and attached to an oil slip table, this shaker was also used to excite the assembly in both the lateral and longitudinal directions.

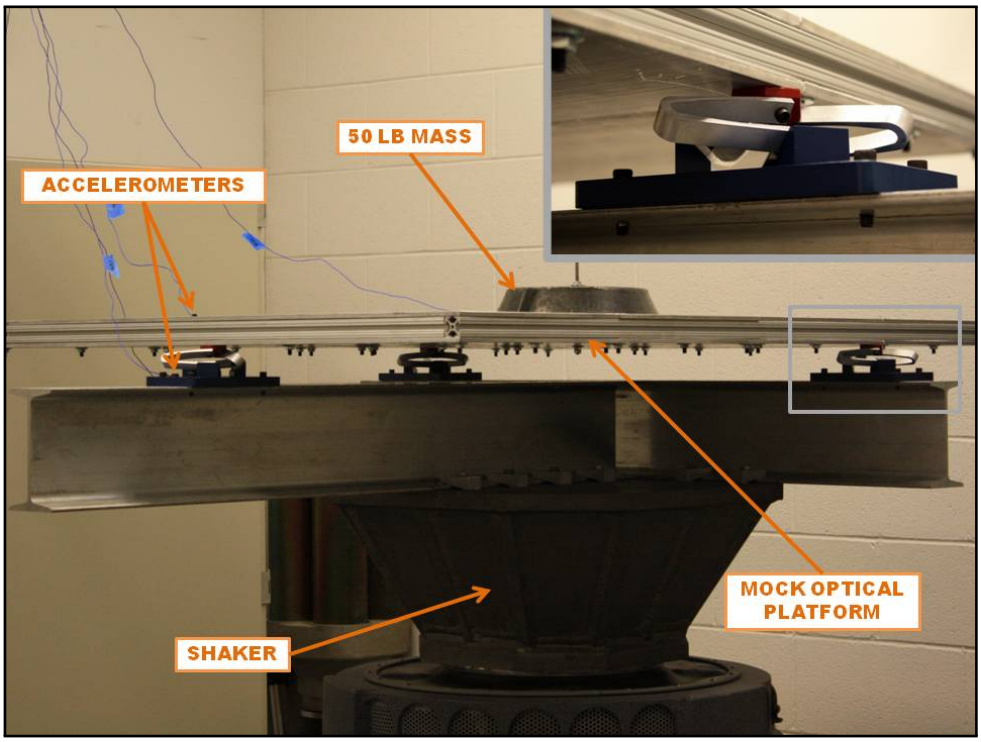

Figure 22 Mock optics platform and isolator assembly on vibration exciter

4. Results and Analysis

4.1 CAD and FE Model

Each design was formulated by creating 3D CAD models. Many of the flaws and design issues were quickly discovered as parts were assembled; however, the behavior of the isolator under load could only be predicted using a FE model. In the case of the isolator design, each part was first designed in CAD and assembled. From the CAD model, a geometrically accurate FE model was created, as shown in Fig. 23. The FE model was used to predict both the static and dynamic response of the isolator assembly to various loads in order to better understand stress distribution. After careful FE analysis, the CAD model was updated to reduce areas of high stress concentration and remove unnecessary material from the springs. The FE model with the final spring shape design is displayed in Fig. 23 with both vertical and lateral displacements of the jewel attachment point. The color contours represent stresses in the materials where the gray jewel is showing the undeformed geometry. Constraints are applied at the bases of the springs where they attach to the pillars and the base plate of the assembly.

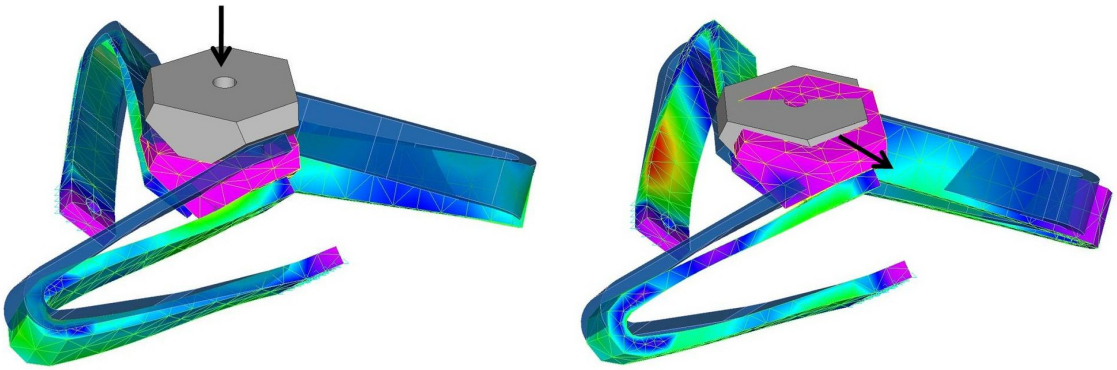

(a) Vertical displacement (b) Lateral displacement

Figure 23 FE model final spring shape analysis with applied static loads

4.2 Stainless Steel Springs

The initial spring material was 316 alloy stainless steel. This material is quite stiff and durable, and as such, it was thought to be necessary for the expected loads. The FE analysis under a static vertical load applied at the jewel attach point is shown in Figs. 24 and 25. As before, the bases of the springs are fully constrained to mimic their attachment to the pillars and base plate. The predicted displacement in inches is shown in the color contours with scale at right. Using the model displacement from the 40 lb static load of 0.0125 in and linearly extrapolating to a 100 lb load, the displacement is predicted to be 0.03125 in. The FE model confirms this linearity with a 100 lb load displacement of 0.313 inches.

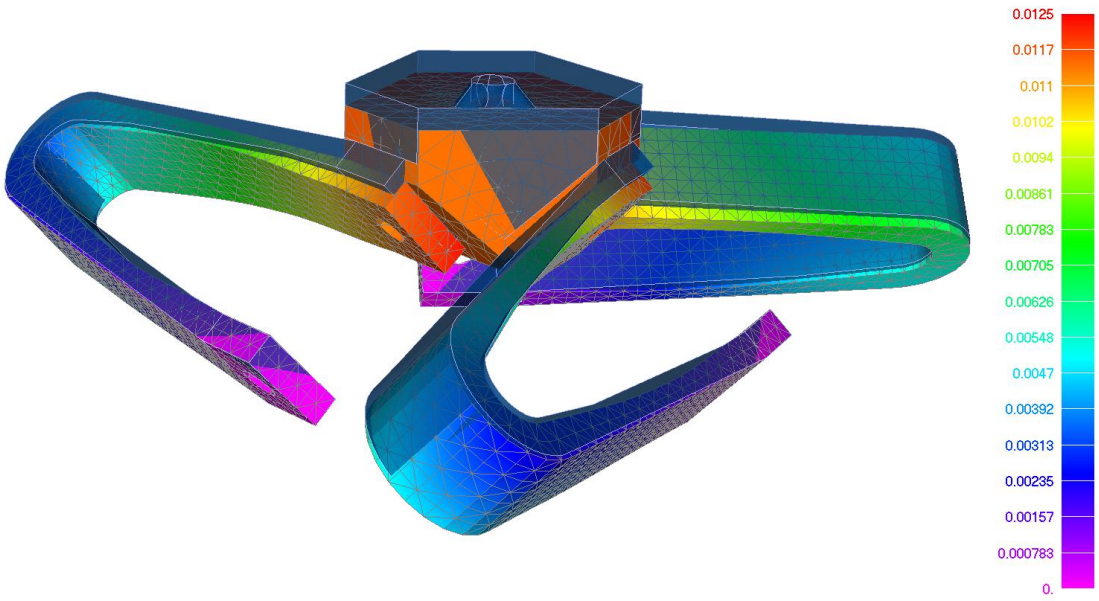

Figure 24 FE model predicted displacements from vertical 40 lb load with stainless steel springs: jewel displacement = 0.0125 in

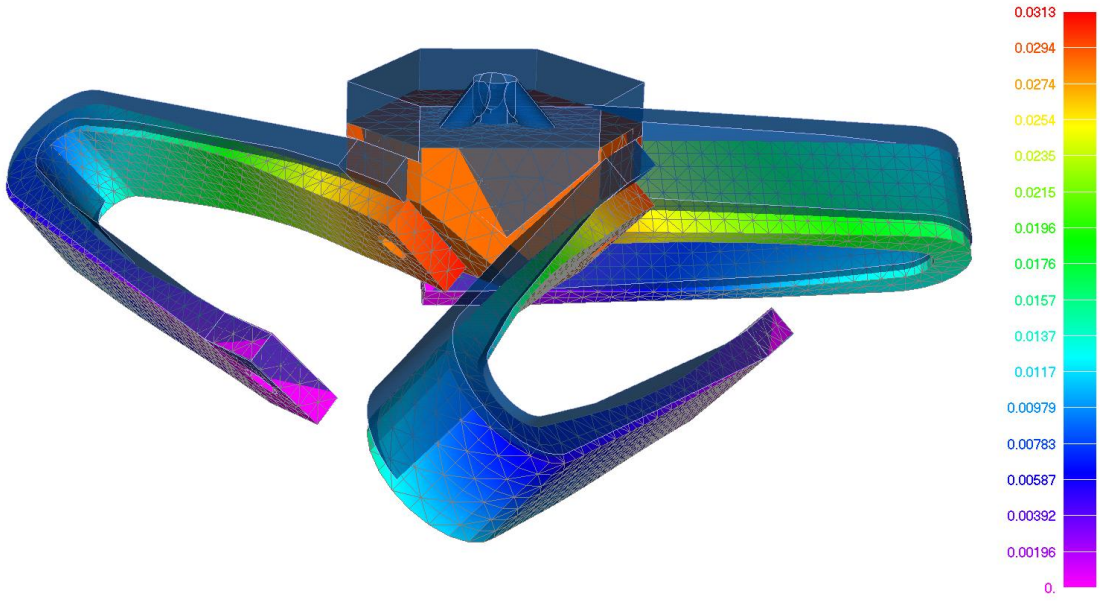

Figure 25 FE model predicted displacements from vertical 100 lb load with stainless steel springs: jewel displacement = 0.0313 in

4.2.1 Static Load Testing. The actual measurements taken in the lab for the various load cases are displayed in Figs. 26–28. The vertical load test results shown in Fig. 26 can be compared to the FE analysis displacement results of Figs. 24 and 25. The opposing lateral load case in Fig. 28 is the same as the lateral load case, Fig. 27, except that the load is now in the opposite direction. Reversing the load was done to see if a particular direction was stiffer and it is as indicated by the steeper slope. Plots of the data accompany the measurement results in graph form. Here a linear regression has been applied to the data and the associated equation and correlation are shown in each plot. Under the loads studied, the isolator assemblies behave very linearly as shown by the FEA. With the static vertical load case of 40 lbs, the FE model differs by 4% and in the 100 lbs load case by only 2% showing excellent correlation.

Load (lb)	Displacement (inch)
20	0.006
30	0.009
40	0.012
50	0.016
60	0.019
70	0.023
80	0.026
90	0.029
100	0.032
110	0.036
120	0.039

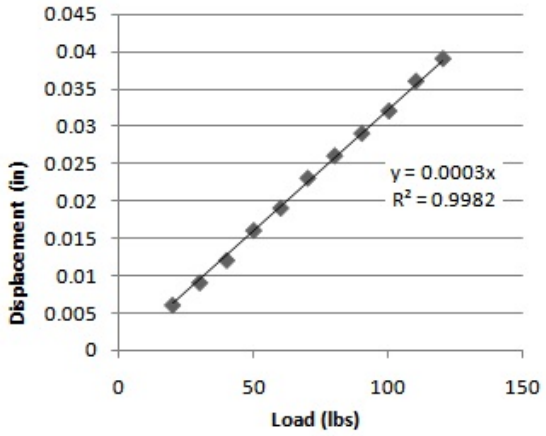

Figure 26 Vertical load test results for stainless steel springs with linear regression

Load (lb)	Displacement (inch)
20	0.008
30	0.011
40	0.015
50	0.020
60	0.024
70	0.029
80	0.033
90	0.039
100	0.045
110	0.053
120	0.060

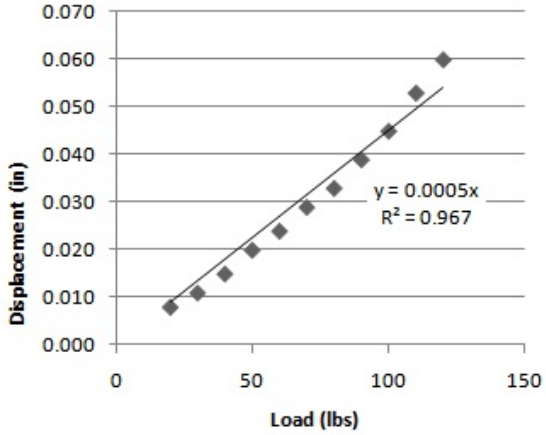

Figure 27 Lateral load test for stainless steel springs with linear regression

Load (lb)	Displacement (inch)
20	0.007
30	0.010
40	0.013
50	0.017
60	0.020
70	0.024
80	0.027
90	0.030
100	0.034
110	0.038
120	0.043

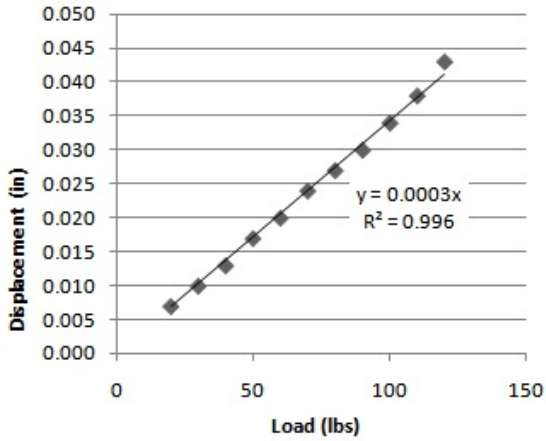

Figure 28 Opposing lateral load test for stainless steel springs with linear regression

4.2.2 Dynamic Testing. An eigenanalysis was performed on the FE model to predict the modes for the first few natural frequencies. The eigenanalysis was completed with a 10 lb mass attached to the jewel which resulted in more realistic modes and natural frequencies of the jewel and springs. Figures 29(a) through 29(f) show the first six modes as predicted by the FE eigenanalysis. The first two modes show mostly a translational motion though due to the spring geometry coupled with a small rotation component. This coupling is present due to the lack of constraint of the attached plate by more than one isolator. Mode three shown in Fig. 29(c) is the torsion mode.

Several tests were conducted using the laser vibrometer to measure velocity and an impulse hammer to provide impulse excitations to the isolator with various masses attached to the jewel. These tests were conducted to validate the FE model's predictions. Though it did appear as though the aforementioned modes are present, it was not possible using only a single laser at a single point to determine the actual mode shape at each natural frequency with high confidence.

It was readily apparent that the steel springs were very stiff and offered little in the way of actual displacement. It was hypothesized that this would cause problems for rubber constrained layer dampers. A quickly constructed set of dampers was applied to the springs to see if this was indeed the case. The results of the dampers in comparison to the undamped isolator is shown in Fig. 30. It can be seen that the rubber does offer a bit of damping by lowering the magnitude and rounding the peak slightly.

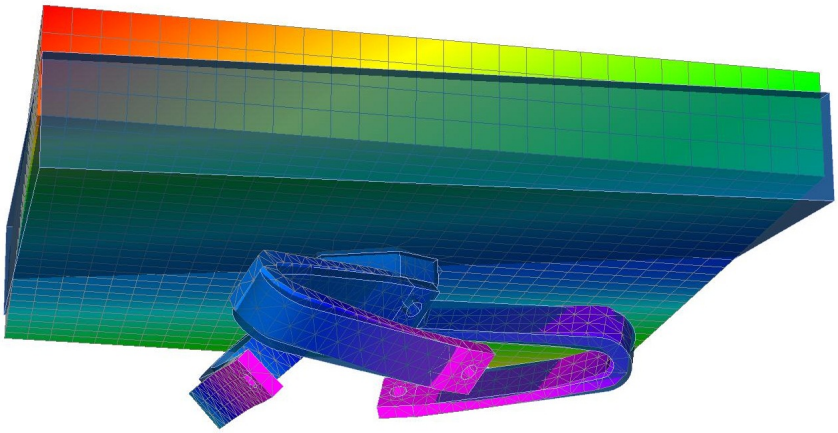

(a) 20.3 Hz mode 1 – first translation/rocking mode

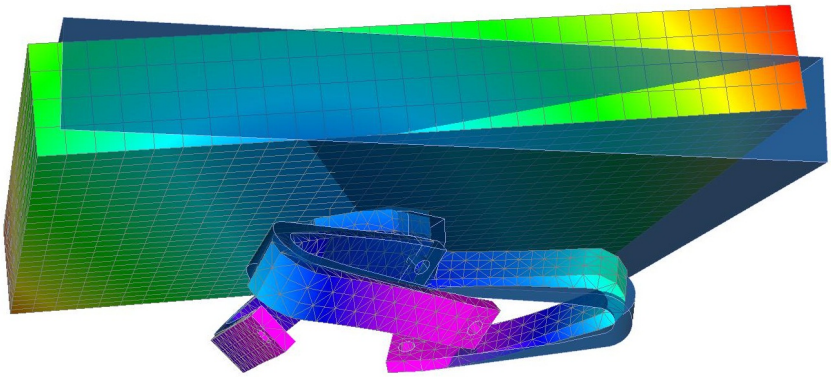

(b) 20.6 Hz mode 2 – second translation/rocking mode

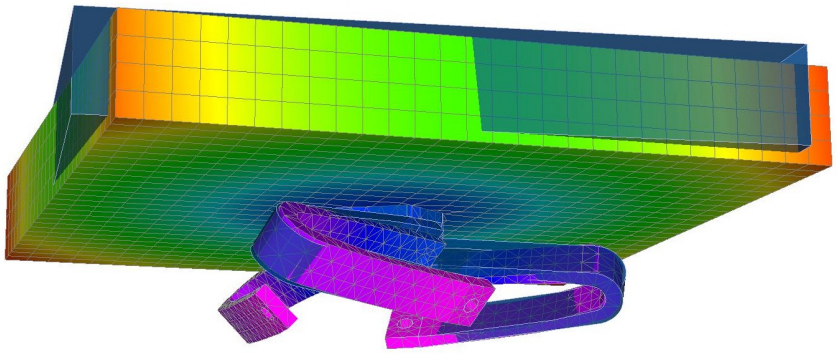

(c) 23.7 Hz mode 3 – first torsional mode

Figure 29 FE model vibration modes of isolator with stainless steel springs with additional 10 lb mass

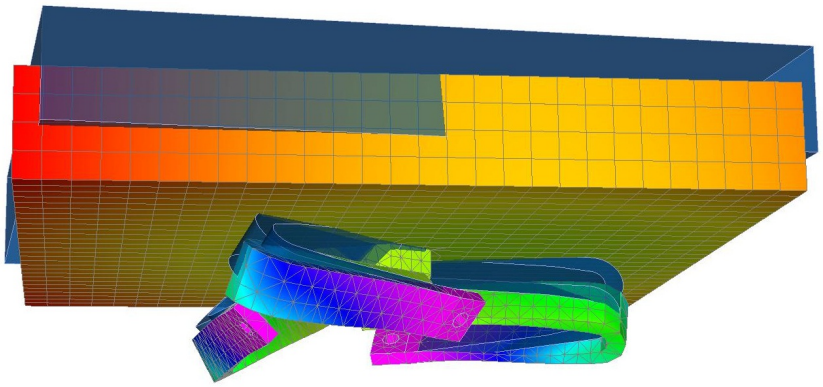

(d) 39.6 Hz mode 4 – pogo or bouncing mode

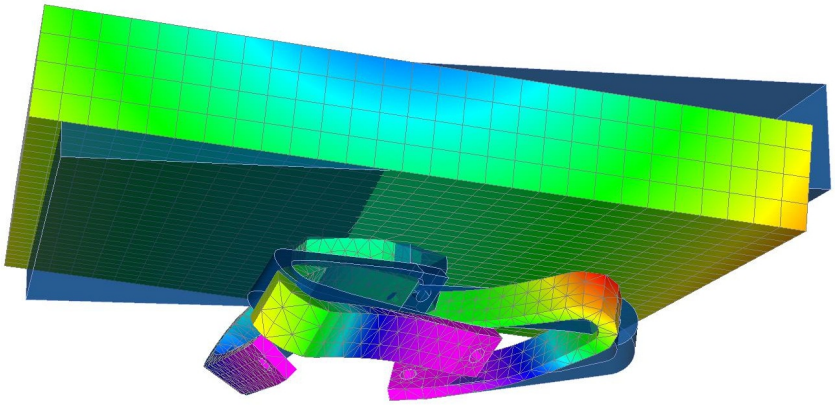

(e) 50.0 Hz mode 5 – third translation/rocking mode

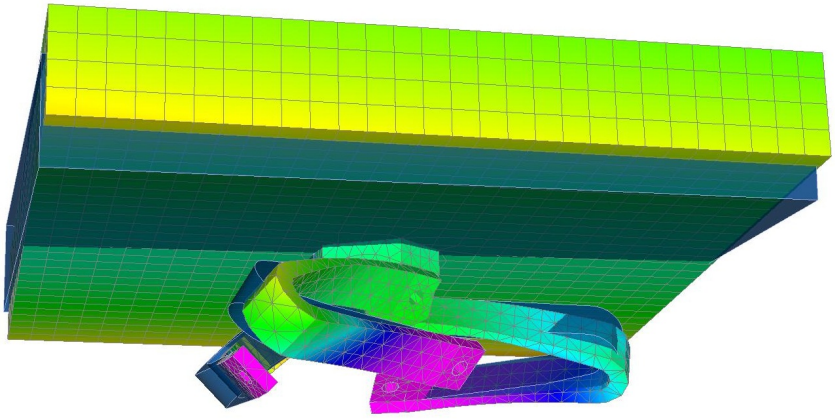

(f) 50.7 Hz mode 6 – fourth translation/rocking mode

Figure 29 FE model vibration modes of isolator with stainless steel springs with additional 10 lb mass

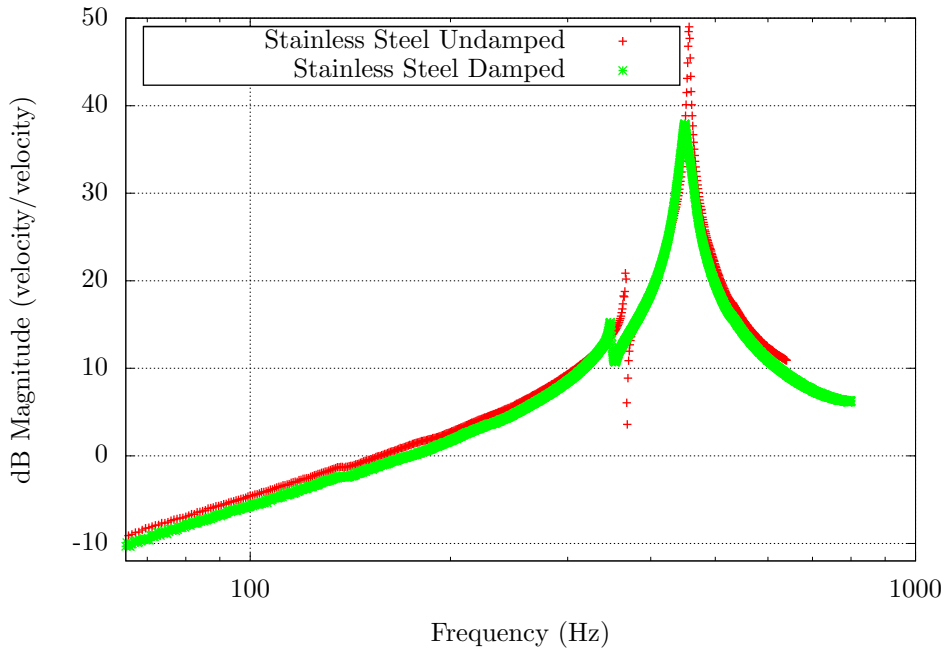

Figure 30 Damping effect with no additional mass and stainless steel springs

4.3 Aluminum Springs

4.3.1 FE Model Extrapolation. As expected, the displacement of the isolator with stainless steel springs was very small. Observing the displacement of the stainless steel springs and the lack of damping, it was decided to soften the springs. The original plan was to only modify the spring shape again using a combination of 3D CAD model changes and viewing the resulting effects through FE analysis. Only changing the shape of the springs quickly proved to be a delicate process and may lead to a spring shape that was not easily manufacturable. Instead, different material properties were swapped out for the springs in the FE model alone until the results appeared to produce a more desirable spring in terms of larger displacements. A readily available 6061 alloy aluminum was chosen and was cut using the same spring shape as the stainless steel springs which saved in fabrication time.

4.3.2 Static Load Testing. The same series of static load tests as conducted on the stainless steel spring isolator were also applied to the the same isolator but

with new aluminum springs. Figures 31–33 show the measured results of the isolator under varying static loads. As before, the data are accompanied by graphical representations. These figures also include linear regressions and their associated parameters are displayed.

Load (lb)	Displacement (inch)
20	0.010
30	0.022
40	0.026
50	0.031
60	0.035
70	0.043
80	0.048
90	0.059
100	0.062
110	0.066
120	0.073
130	0.076
140	0.081
150	0.083

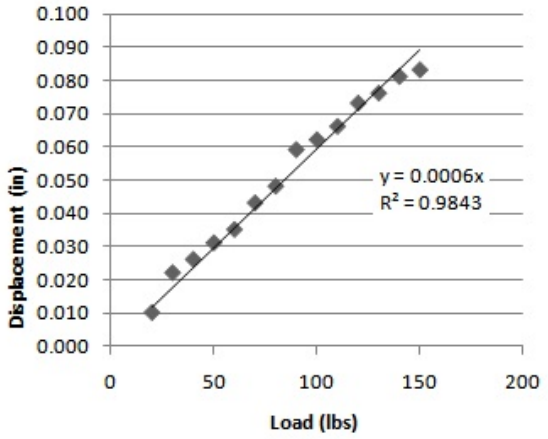

Figure 31 Vertical load test for aluminum springs with linear regression

Load (lb)	Displacement (inch)
20	0.012
30	0.022
40	0.028
50	0.035
60	0.040
70	0.048
80	0.055
90	0.060
100	0.068
110	0.074
120	0.081
130	0.089
140	0.095
150	0.100

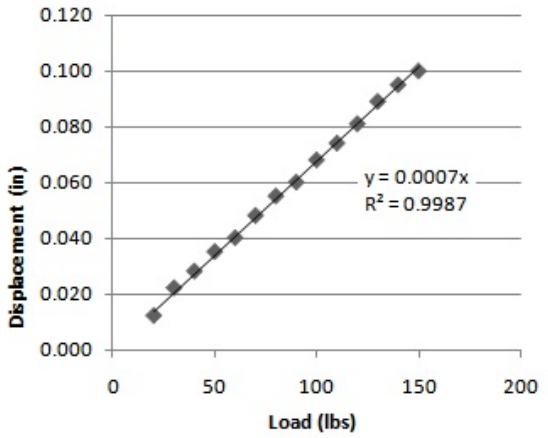

Figure 32 Lateral load test for aluminum springs with linear regression

Load (lb)	Displacement (inch)
20	0.008
30	0.013
40	0.018
50	0.022
60	0.026
70	0.030
80	0.034
90	0.038
100	0.042
110	0.045
120	0.048
130	0.052
140	0.055
150	0.059

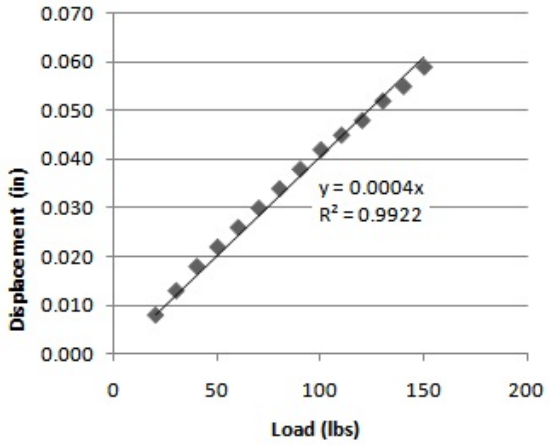

Figure 33 Opposing lateral load test for aluminum springs with linear regression

4.3.3 Dynamic Testing. Several dynamic tests using a laser vibrometer were again conducted to aid in characterizing the isolator. Overall, the same FRFs were measured with aluminum springs as with the stainless steel springs to collect velocity measurements. By collecting the same responses, a direct material comparison can be made since the physical dimensions and shape of the springs and isolator did not change. Most importantly, though, is the comparison of the rubber dampers with the two different spring materials. These data are shown in Fig. 34.

Notice that the rubber application to the stainless steel springs resulted in a reduction of approximately 11 dB whereas with the aluminum, the reduction is close to 24 dB. The damped peak associated with the aluminum springs is also much broader indicating that the damping is much more effective with the larger displacements. It should be noted, however, that the damped peak of the aluminum has shifted to the right towards a higher frequency which is contrary to pure damping. It is seen here that the rubber dampers as applied to the sides of the aluminum is increasing the stiffness of the isolator system which is not necessarily desirable. It does not appear that this slight shift in natural frequency is going to adversely effect the performance of the isolator.

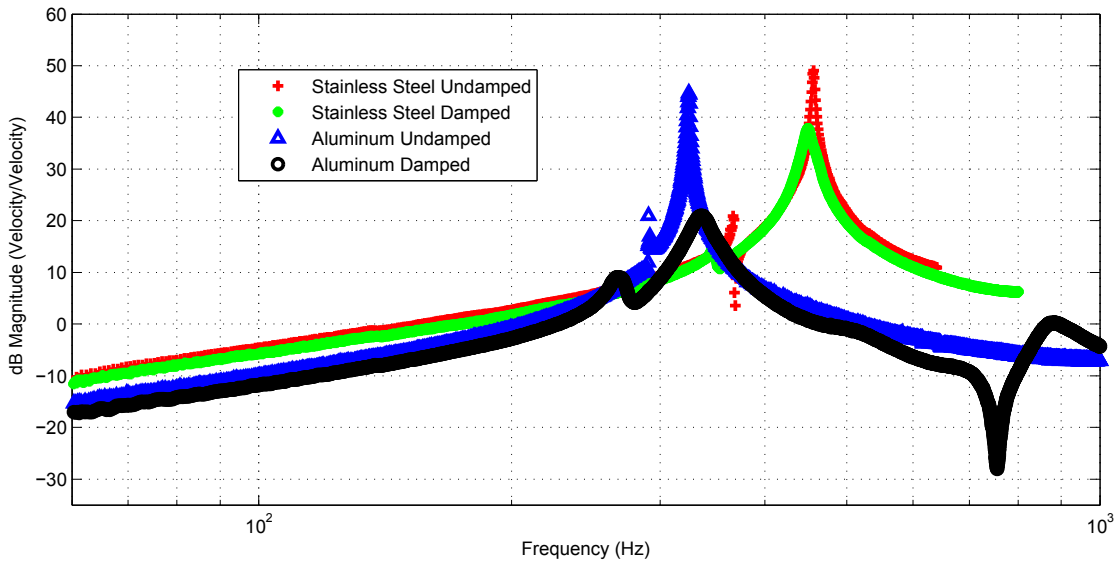

(a) Full test spectrum

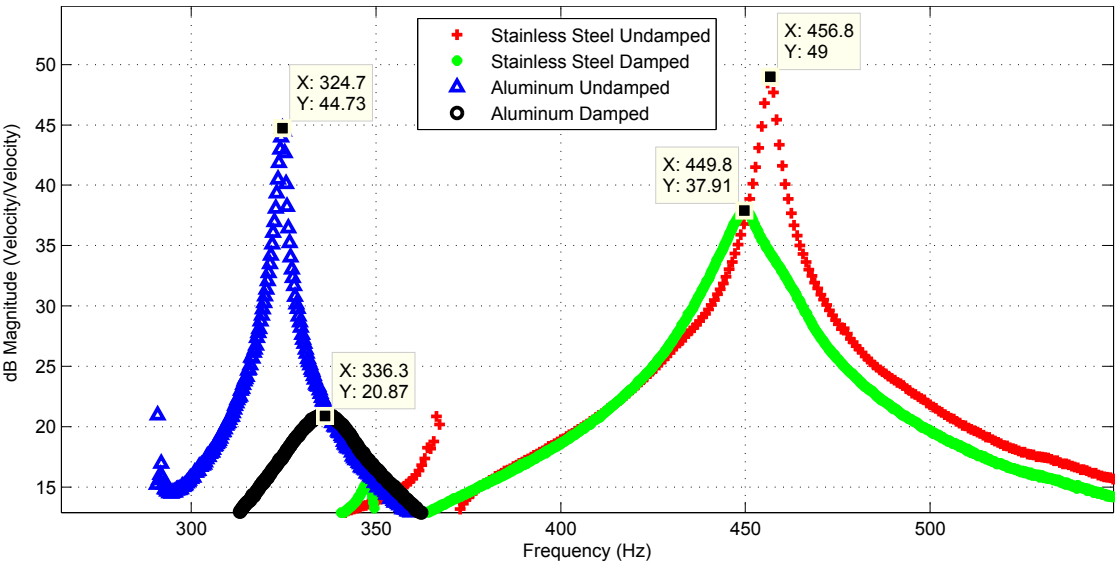

(b) Peak detail

Figure 34 Single isolator with no additional mass attached

4.4 Damping Effects

The original damper material was hand cut from an aircraft rubber inner tube rubber and applied to a similarly cut sheet of aluminum. Two such rubber dampers were adhered to either side of each spring using the neoprene adhesive and held in place with two through bolts. The dampers were used on the single isolator as mentioned above for dynamic testing with the laser vibrometer. The same dampers were applied with both the stainless steel and aluminum spring sets to compare. However, being hand cut from scrap rubber, the dampers were not ideal to be replicated for the three additional isolators used to support the mock optical platform.

New rubber materials were purchased and fabrication methods were created. Two types of rubber were purchased with what were thought to be similar properties of the butyl rubber found in the inner tube. These two rubbers, Neoprene and Buna-N, were cut with a water jet machine and placed on the single isolator used before with the laser vibrometer. This isolator and damper setups were tested using the vibration exciter with 30 lbs additional mass attached to the jewel. Both rubber materials were tested each with and without through bolts. It was determined that the Neoprene with the through bolts was the best candidate for further testing due to observed indications of better damping.

The sine sweep frequency response in Fig. 35 is the frequency response of the isolator with neoprene permanently adhered and through bolts applied for the damped case. The test, shown previously in Fig. 21, was conducted at two different acceleration levels with and without the damping. Figure 35(b) shows a close up of the peaks. An interesting phenomenon is noted here. The two peaks on the left are the undamped cases whereas the peaks on the right have the damping applied. This is contrary to the effects expected for damping alone. The increased resonance frequency shows that the dampers are adding stiffness to the system. Also interesting is the lower peaks (both left and right) are the result of the higher base input excitation. It follows from this test that more damping is observed at high input

levels with and without the dampers in place. It appears, then, that there is a significant amount of non-linear damping with respect to input magnitude due to the material effects in this particular geometry.

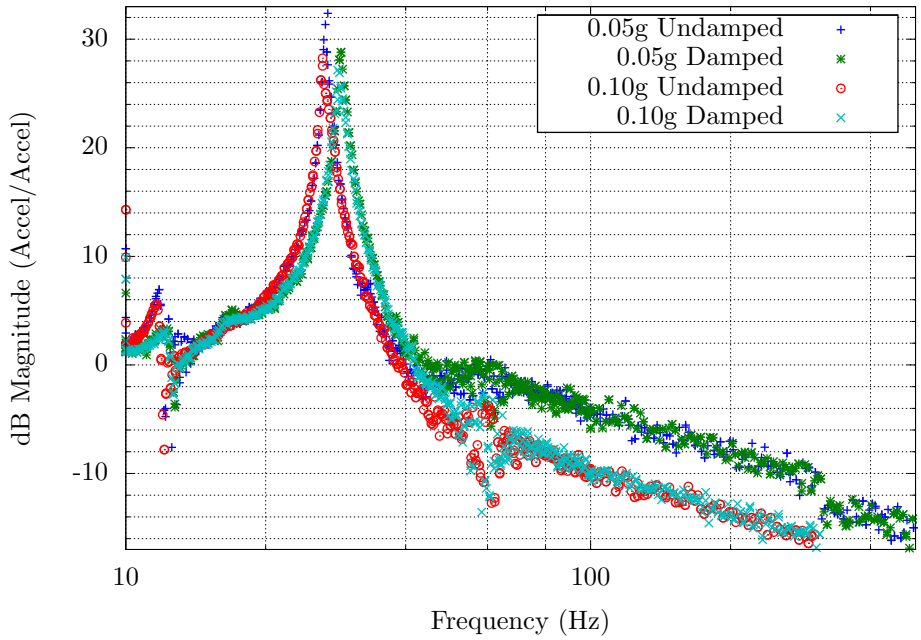

(a) Full test spectrum

Figure 35 Vibration exciter sine sweep of single isolator with 30 lbs additional mass attached

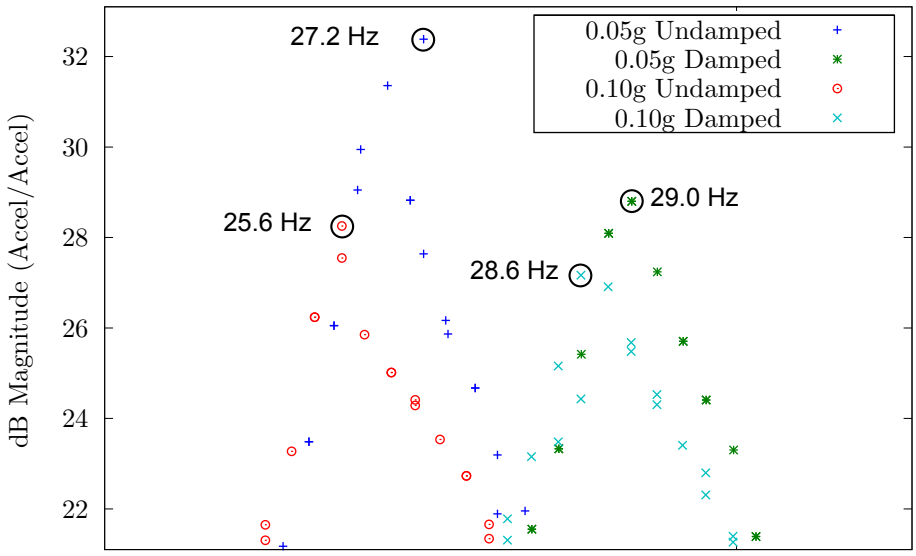

(b) Peak detail

Figure 35 Sine sweep of single isolator with 30 lbs additional mass attached

4.5 Mock Optics Platform Assembly

4.5.1 Sine Sweep Characterization. The sine sweep on the vibration exciter is the simplest test input used to characterize a given system. Here, the attempt is to define the transfer function from the base attachment structure through an individual isolator to the mock optical platform. The assembly was characterized by exciting in three orthogonal directions: lateral, longitudinal, and vertical. The lateral and longitudinal excitations were performed on the horizontal slip table with the longitudinal direction being the long dimension of the breadboard. The vertical excitation was conducted with the assembly on top of the shaker head. The results of the sine sweeps in these three configurations are shown in Figs. 36, 37, and 38.

Both the damped an undamped cases are shown. These are acceleration data and, save for the vertical results, display the characteristic approach, peak(s) and an approximately 40 dB/dec cutoff beyond resonance. There vertical result data do not show the desirable cutoff beyond the resonant point. This phenomenon can not be

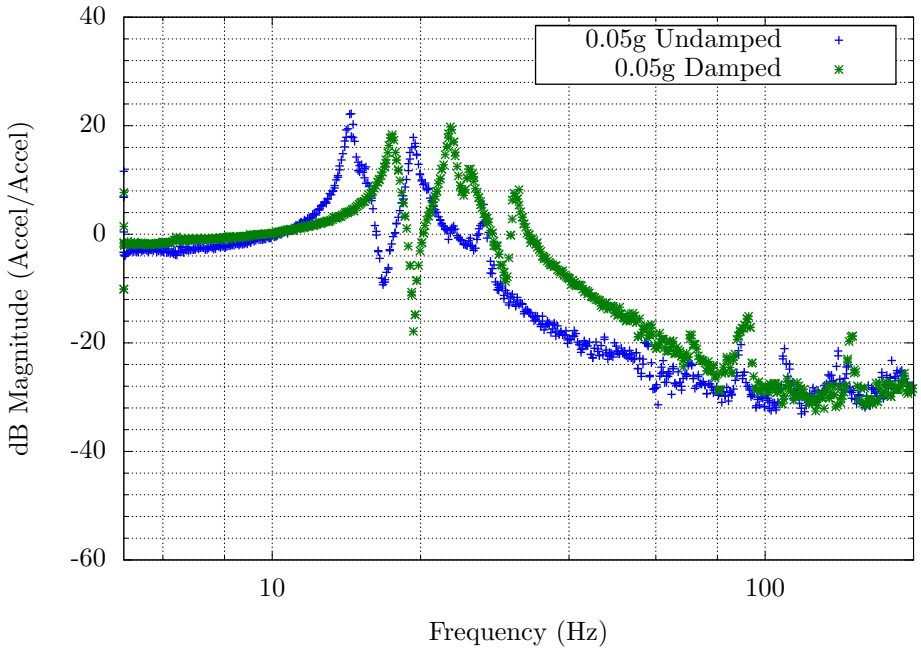

Figure 36 Lateral sine sweep of a single isolator attached to the breadboard assembly

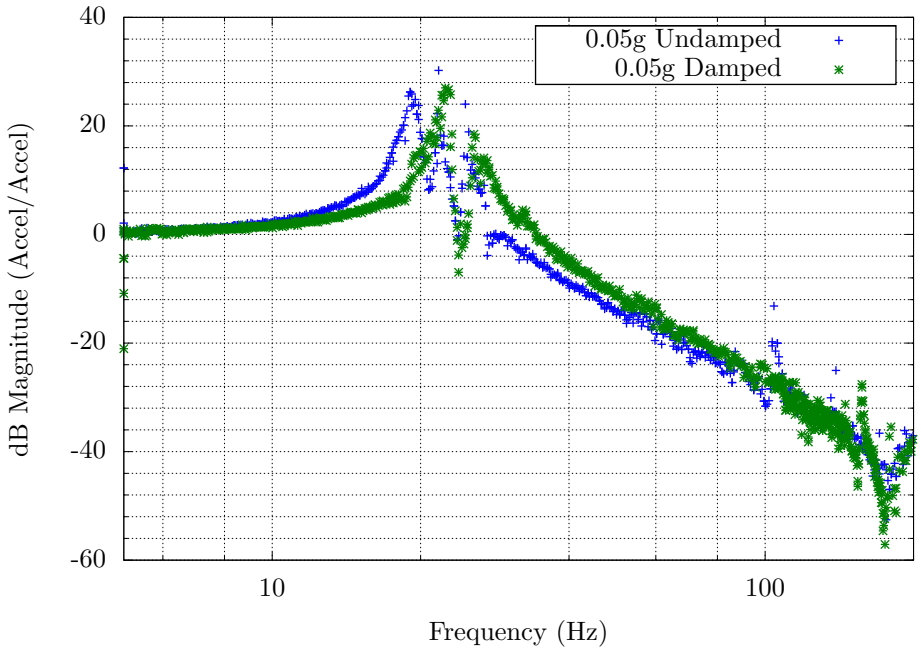

Figure 37 Longitudinal sine sweep of a single isolator attached to the breadboard assembly

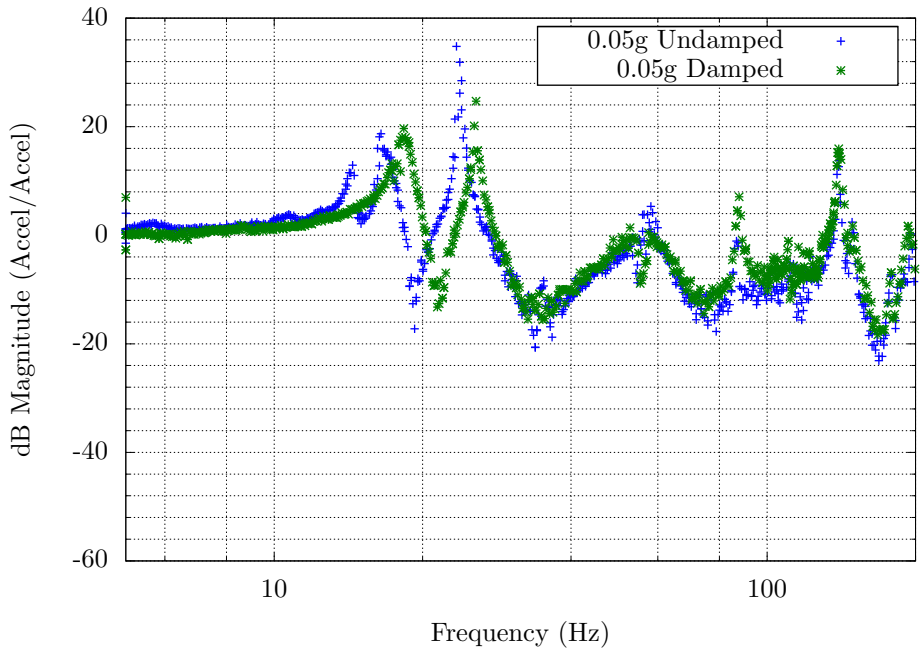

Figure 38 Vertical sine sweep of a single isolator attached to the breadboard assembly

completely explained as the data here are taken from an accelerometer directly atop an isolator with respect to an accelerometer attached to the base of that isolator eliminating any undesirable effects of the support structure or optical platform's dynamic characteristics. Tightness of the screws in the isolator assembly were also checked between the damped and undamped cases of the vertical excitation and were found to be consistent.

4.5.2 Breadboard Damping Effects. In general, the lack of additional damping provided by the rubber dampers as applied with the breadboard assembly were not as desired. In all of the above damping test cases, the results show that the dampers indeed add more to the stiffness of the system than they add to the damping. In fact, little to no additional damping is observed when the isolators are part of the mock optics platform assembly. The vibration exciter results thus far do show that there may be some dependence on the input acceleration level.

It appears from the sine sweep, random vibration data, and from physically observing the motion of the platform during vibration testing on the exciter that there may indeed be far too much displacement at the resonances with respect to the shaker. This large displacement seems to indicate that the capability of the rubber to provide damping from shear stresses is being exceeded and the rubber is only functioning as an additional spring. From tests with the laser vibrometer with no additional mass on the isolator, as previously shown in §4.3.3, the rubber dampers did in fact add to the damping of the system and only slightly to the overall stiffness. Because of this, it was desired to attempt a much lower level test excitation to determine if this better damping regime could be found for the breadboard and isolator assembly.

4.5.3 Random Vibration. Due to the concern of higher level acceleration effects and knowing that the vibration environment aboard the ISS is extremely low, it was decided to conduct a random vibration test. This test can be performed at much lower acceleration levels than the sine sweep though it is more difficult and time consuming to setup and test. For this reason, only a vertical random vibration was conducted in order to determine whether the performance of the isolators varied at these lower levels. The results of this test are shown in Fig. 39. For a control, the 0.03g and 0.05g levels of the sine sweeps were repeated here. It is clear from this test that though there is some variation between excitation levels in small frequency bands, overall there is no significant dependence on acceleration magnitude within this range.

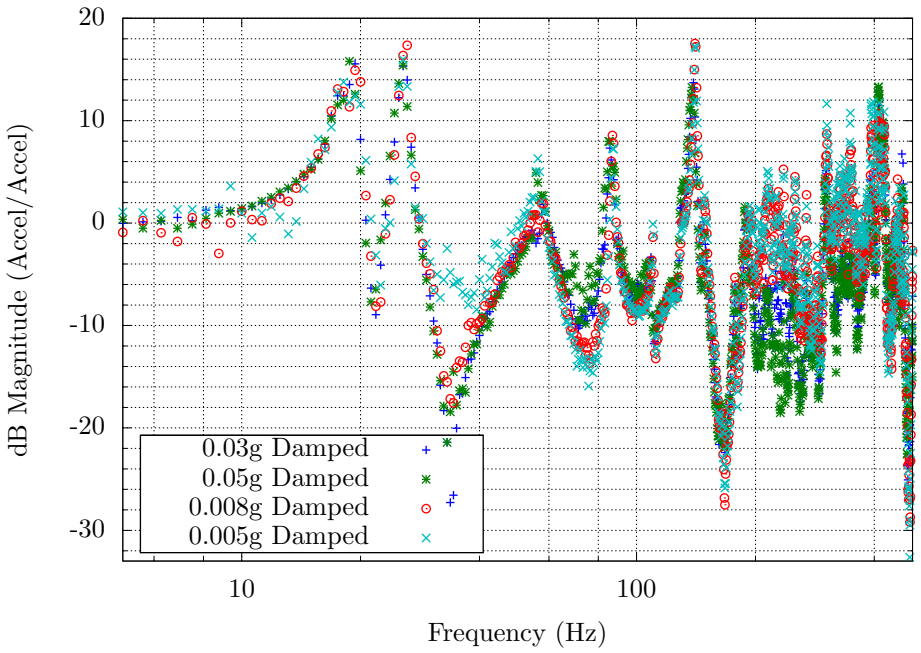

Figure 39 Vertical random vibration of a single isolator attached to the breadboard assembly

5. Conclusions

5.1 Overall Design and Test

The goal of the design was to provide multi-degree of freedom vibration isolation and suppression in a compact form for use in space applications. The subjects of 3D isolation and compact design are typically trade-offs whereas both are beneficial and important in space applications. Most imaging systems require a very stable platform and demand more than what a simple 1D isolator can provide. However, using large amounts of space for a full hexapod-like design when considering launch and vehicle costs is a difficult trade space in which a designer has to work. The triple isolator meets the goal of allowing motion in any direction or rotation and is very compact compared to larger hexapod type designs. The design, fabrication, and test of the isolators and the mock optical platform was completed in approximately seven weeks time which resulted in several time saving techniques such as preserving spring shapes when switching from stainless steel to aluminum.

The results of the experimental vibration analysis match the predicted behavior of the FE model. The FE model was tuned for the stainless steel springs for both static loads and dynamic analysis. The model was not tuned for either case with the aluminum springs nor was a FE analysis completed for the entire assembly of isolators and mock optical platform. This is a good starting point for better understanding the behavior of the isolators while attached to a larger system where they are designed to work. This should be done prior to any different approach to passive damping or in consideration for an additional active control system if desired.

The isolator geometry is such that it can easily be varied to eliminate the stiffness directionality of the assembly. Currently, the lateral and vertical translations do not exactly match in terms of natural frequency. However, varying the angle at which the springs are attached to the pillars and jewel (currently 45°) will bring these closer together. Similarly, translational and rotational motion of the jewel is coupled

with spring cross-section. Adjusting the width to thickness ratio of the spring cross-section may be used to either bring the rotational mode frequencies closer to those of the translational modes or further separate them. Together, these properties allow this isolator to be customized to any particular application.

5.2 Damping Considerations

Research and study of methods for providing damping to this design is by far the most important area for improvement. The simple rubber dampers experimented with at this point are not ideal offer little to the overall design goal. The results of the numerous experiments do indeed conclude that this damping technique is not practical for higher levels of acceleration though it was important to eliminate this option as it is by far the simplest approach to passive damping with this geometry.

It is still not entirely clear as to why the dampers appear to offer some significant level of damping when tested with no attached mass using the laser vibrometer and a calibrated impulse. However, when used with the vibration exciter setups, the dampers failed to provide measurable damping but rather their application resulted in additional system stiffness. Some tests seemed to indicate that the opening/closing motion of the springs if minimal compared to their sideways motion. This would explain the results of the rubber dampers applied at the sides and would suggest that the sideways motion be analyzed next. As indicated by the FE analysis, There is no pure, simple directional motion of any spring. That is, no spring simply opens and closes, or is torqued inducing lateral separation, but rather, each movement is some complex combination of these and other modes.

One possible approach would be to fill the area inside each spring and between the existing rubber constrained layer dampers with a viscoelastic material. Another idea is to encapsulate the entire spring in such a material preferably in a fluid form that would harden around the spring providing damping with any motion. This would be a bulky method and would require a large amount of rubber material to

be added to the design. A final, and likely best approach would be a laminated spring structure. This would entail several layers of metal and viscoelastic material to "build up" the spring's thickness; however is most difficult to fabricate.

5.3 Space Application

All space applications involve vibration that are not readily damped by their environment as they are on Earth which opens a very large door for vibration isolation and suppression systems in space work. Vibrations in space structures result from several origins such as spinning components used for pointing and stabilization as well as attitude control thrusters for orbital maneuvers. Each such vibration remains with the spacecraft for long periods of time unless actively removed.

Numerous satellites, as well as manned spacecraft, have payloads which demand certain pointing constraints. These include sensitive high gain radio antennae, cameras, microgravity research experiments, thematic mappers, Earth weather instruments and many more. At this point in time, either small linear isolation devices or large arrangements of isolators for multiple degrees of freedom have been implemented for these types of systems usually at much cost in weight, space and active control systems. The compact triple isolator's goal is to reduce these burdens to the spacecraft designer.

It will be key to look at the materials used in the final construction of the triple isolator. Many materials are not approved for space applications especially in optically sensitive environments like the chromotomographic imager experiment. These materials, like the neoprene rubber currently being used for the constrained layer damping approach, will out-gas in vacuum and cloud the optical components restricting the usability of the equipment. Other materials may pose mechanical problems after longer times exposed to the space environment. At no point during the design of this isolator experiment were these material considerations taken into account save for the knowledge that the current choices would not be suitable for

space application. It was decided that in order to save considerable time and money, the geometry and application of such materials to the isolator design would take precedence and applicable materials having similar properties would be substituted for space application once finalized. A by product of this approach is an isolation system that is still inexpensive and usable in similar Earth applications.

5.4 Future Work

The isolator design is at a good starting point for continued work towards designing compact isolators with good damping and isolation properties. The design has proven that the spring geometry can be used to allow for multidirectional isolation in a compact and inexpensive design. There are a few aforementioned ideas that have simply not had the time to be tested with the isolator in its current configuration. Numerous other techniques could be attempted to include modification of the overall spring assembly's geometry.

Another future work item is the application of some means of active control. It was the goal to find a system that could meet the requirements of the CTEx without needing active control, however, further developing this area could result in even larger applications of the triple isolator. Several ideas of active control have been surmised to include piezoelectric patches applied to the springs with a three axis accelerometer attached to the lower point on the jewel. Other concepts include methods of attaching linear actuators between the jewel and the base plate to accomplish a similar task of controlling the damping characteristics electronically.

A final area of study is necessary in terms of launch isolation. The triple isolator design saves room beneath the jewel to which a frangible bolt could be attached for purposes of securing the payload during launch. This area, though, has not been looked at systematically and requires more investigation. This isolation system is not designed to provide for both on-orbit and launch vibration control. These two areas are both vitally important, however, these characteristics, mostly in terms of

acceleration magnitudes, are wildly different and can not at this time be properly addressed using a single configuration.

Appendix A. MATLAB Analysis Code

A.1 Laser Vibrometer Data Analysis

```
function showData()
clear all; close all; clc;
global figs;
figs = 0;

    function plotData(fileName, lineColor, legendText, plotTitle)
        % plotData(string fileName, string lineColor, string legendText
        % [, string plotTitle])

        H = load(fileName, 'H1_2');
        H = [H.H1_2(:,1) 20*log10(abs(H.H1_2(:,2)))];
        if (nargin == 4) % create new plot if plot title is specified
            fullscreen = get(0, 'ScreenSize');
            figure('Position', [.05*fullscreen(3) .1*fullscreen(4)...
                .9*fullscreen(3) .8*fullscreen(4)]);
            figs = figs + 1;
            semilogx(H(:,1),(H(:,2)),lineColor, 'LineWidth', 2);
            title(['Transfer Function - ' plotTitle]);
            xlabel('Frequency (Hz)')
            ylabel('Magnitude (dB)');
            hold on;
            grid on;
        else % add to the existing plot
            plot(H(:,1),(H(:,2)),lineColor, 'LineWidth', 2);
        end
        % append legend text to the current plot
        [legend_h,object_h,plot_h,text_strings] = legend;
        text_strings{end+1} = legendText;
        legend(legend_h,text_strings,'location','Best');

        % point to the max peak
%         [maxVal, maxInd] = max(abs(H(:,2)))
%         maxLoc = H(maxInd,1)
%         currentAxis = axis
%         xend = (maxLoc - currentAxis(1))/(currentAxis(2) - currentAxis(1)) % normaliz
%         yend = (maxVal - currentAxis(3))/(currentAxis(4) - currentAxis(3))
%         xbegin = xend
%         ybegin = yend + 0.05
%
%         ann_h = annotation('textarrow',[xbegin xend], [ybegin yend]);
%         set(ann_h,'String',[num2str(maxLoc) ' Hz'])
    end % plotData

% basic isolator with no mass
% saved as IsolatorWithNoMassZoom.eps/pdf
```

```
% saved as IsolatorWithNoMass.eps/pdf
plotData('TripleIsolator', '+r', 'Stainless Steel Undamped', 'Isolator with No Mass');
plotData('IsolatorDamped', '*g', 'Stainless Steel Damped');
plotData('AlumIsolator', '^b', 'Aluminum Undamped');
plotData('AlumIsolatorCDamp2', 'ok', 'Aluminum Damped');
axis([60 600 -13 60]);
%legend('Stainless Steel Undamped','Stainless Steel Damped', 'Aluminum Undamped','Alumi

% steel isolator with 10 lbs for model comparison NOT FOUND
plotData('Alum50lbs', '+r', 'Alum50lbs', 'Isolator with 10lbs Mass');
plotData('Alum10lbsCorner', '*g', 'Alum10lbsCorner');
plotData('50lbsMass', '^b', '50lbsHighRes');
plotData('10lbsSide', 'ok', '10lbsSide');
axis([0 60 -20 60]);

% 50 lbs with center sensor
plotData('50lbsMass', '+r', 'Stainless Steel Undamped',...
    'Isolator with 50lb Mass');
plotData('50lbsDampedClamped', '*g', 'Stainless Steel Damped');
plotData('Alum50lbs', '^b', 'Aluminum Unamped');
plotData('Alum50lbsCenterCDamp2', 'ok', 'Aluminum Damped');
axis([0 50 -60 60]);

% Damped center bolt sensor
plotData('Alum10lbsCenterCDamp2', '+r', '10lb Mass',...
    'Damped Aluminum Isolator with Mass Center Measurement');
plotData('Alum50lbsCenterCDamp2', '^g', '50lb Mass');
axis([0 180 -30 30]);

% Stainless damping comparison
plotData('TripleIsolator', '+r', 'Stainless Steel Undamped', 'Isolator with No Mass');
plotData('IsolatorDamped', '*g', 'Stainless Steel Damped');


% reverse figure display order so that 1 is on top
for ctr = linspace(figs,1,figs)
    figure(ctr)
end

end % showData
```

```
function showData(dataSet)
%
%       showData(DATASET)
%
%       DATASET specifies which analysis case number to run from assignData.m or
%         '?' to view available cases
%
% This program written to display data collected from the breadboard and isolator
% setup. Data from each sensor of each run are saved as individual ascii *.ASC files.
% This program is optimized for Octave. Steven D. Miller 21 Jan 2010
%
%

warning('off','Octave:load-file-in-path');
warning('off','Octave:fopen-file-in-path');

% check to see that the input argument was specified
if (nargin ~= 1)
    dataSet = input('Please specify an analysis set number or ? for options: ', 's');
end

% show options
if (dataSet == '?')
    num = 1;
    while (num > 0)
        [display, legendText, titleText] = assignData(num);
        if (titleText == 0)
            num = 0;
        else
            disp(sprintf('%3.0f --- %s', num, titleText));
            for ctr = 1:size(legendText,1)
                disp(['             ' legendText(ctr,:)]);
            end
            num = num + 1;
        end % if
    end % while
    disp(' ');
    return;
elseif (ischar(dataSet))
    dataSet = str2num(dataSet);
end

[display, legendText, titleText] = assignData(dataSet);

if (titleText == 0)
    disp('Not a valid DATASET. Check assignData.m for valid analysis cases.');
    return;
end
```

```
49
50 % set line markers
51 markers = ['+', '*', 'o', 'x', '^'];
52 %markers = '-';
53 numMarkers = length(markers);
54 markerCtr = 1;
55
56 % begin assembling the plot command
57 plotCommand = "semilogx(";
58
59 % cell array to store the data read from the files
60 data = cell(size(display,1));
61
62 for ctr = 1:size(display,1)
63     run = display(ctr,1);
64     input = display(ctr,2);
65     output = display(ctr,3);
66
67     % get the data from the files
68     if (input == 0) % don't divide by input data
69         outFile = ['R' num2str(run) '_S' num2str(output) '.ASC'];
70         outData = load(outFile);
71         %disp(['Loaded ' outFile]);
72         data(ctr) = outData(:,2:3); % col 2 = freq; col 3 = mag
73     else % divide by the input
74         inFile = ['R' num2str(run) '_S' num2str(input) '.ASC'];
75         outFile = ['R' num2str(run) '_S' num2str(output) '.ASC'];
76         inData = load(inFile);
77         outData = load(outFile);
78         %disp(['Loaded ' inFile]);
79         %disp(['Loaded ' outFile]);
80
81         % fix input and output data lengths by truncating longer data
82         inPoints = size(inData,1);
83         outPoints = size(outData,1);
84         diff = outPoints - inPoints;
85         if (diff > 0)
86             outData(end-diff+1:end,:) = [];
87         elseif (diff < 0)
88             inData(end+diff+1:end,:) = [];
89         end
90         normMag = outData(:,3)./inData(:,3);
91         data(ctr) = [outData(:,2), normMag];
92     end
93
94     % assemble the plot command
95     plotCommand = [plotCommand  'data{' num2str(ctr) '}(:,1), data{' num2str(ctr) "}(:,
96     if (markerCtr == numMarkers)
97         markerCtr = 1;
98     else
99         markerCtr = markerCtr + 1;
```

```
100     end
101
102     % convert to dB
103     data{ctr}(:,2) = 20*log10(data{ctr}(:,2));
104 end
105
106 % finish the plot commnd by replacing the last comma with a )
107 figure();
108 plotCommand(length(plotCommand)) = ')';
109 eval(plotCommand);
110 title(titleText);
111 xlabel('Frequency (Hz)');
112 ylabel('Magnitude (dB)');
113 legend(legendText);
114 grid('minor', 'on')
115
116 end
```

```
function [display, legendText, titleText] = assignData(dataSet)
% Some senors should be divided by others to properly create the FRF
% Assign which input/output pairs should be displayed
% each row is an input – output pair
% specify input num = 0 to not divide the output
% [input run num, input sens num, output sens num]

switch dataSet

case 1
    display = [...
        27 1 2;
        25 1 2;
        26 1 2;
        24 1 2;
    ];

    legendText = [...
        '0.05g Undamped',
        '0.05g Damped',
        '0.10g Undamped',
        '0.10g Damped'
    ];

    titleText = ['Frequency Response Function – Single Isolator + 30 lbs'];
    return;

case 2
    display = [...
        28 1 2;
        28 3 4;
        29 1 2;
        29 3 4;
        30 1 2;
        30 3 4;
        31 1 2;
        31 3 4;
    ];

    legendText = [...
        '0.03g Center Breadboard',
        '0.03g Isolator A',
        '0.05g Center Breadboard',
        '0.05g Isolator A',
        '0.075g Center Breadboard',
        '0.075g Isolator A',
        '0.1g Center Breadboard',
        '0.1g Isolator A'
    ];

    titleText = ['Frequency Response Function – Breadboard + 50 lbs, undamped, vertical
```

```
52      return;
53
54  case 3
55      display = [...
56          28 1 2;
57          29 1 2;
58          30 1 2;
59          31 1 2;
60      ];
61
62      legendText = [...
63          '0.03g Center Breadboard',
64          '0.05g Center Breadboard',
65          '0.075g Center Breadboard',
66          '0.1g Center Breadboard'
67      ];
68
69      titleText = ['Frequency Response Function – Breadboard + 50 lbs, undamped, vertical
70      return;
71
72  case 4
73      display = [...
74          28 3 4;
75          29 3 4;
76          30 3 4;
77          31 3 4;
78      ];
79
80      legendText = [...
81          '0.03g Isolator A',
82          '0.05g Isolator A',
83          '0.075g Isolator A',
84          '0.1g Isolator A'
85      ];
86
87      titleText = ['Frequency Response Function – Breadboard + 50 lbs, undamped, vertical
88      return;
89
90  case 5
91      display = [...
92          32 3 4;
93          33 3 4;
94          34 3 4;
95          35 3 4;
96      ];
97
98      legendText = [...
99          '0.03g Isolator C',
100         '0.05g Isolator C',
101         '0.075g Isolator C',
102         '0.1g Isolator C'
```

```
103     ];
104
105     titleText = ['Frequency Response Function — Breadboard + 50 lbs, undamped, longitud
106     return;
107
108 case 6
109     display = [...
110         36 3 4;
111         37 3 4;
112         38 3 4;
113         39 3 4;
114     ];
115
116     legendText = [...
117         '0.03g Isolator C',
118         '0.05g Isolator C',
119         '0.075g Isolator C',
120         '0.1g Isolator C'
121     ];
122
123     titleText = ['Frequency Response Function — Breadboard + 50 lbs, undamped, lateral'
124     return;
125
126 case 7
127     display = [...
128         7 0 2;
129         4 0 2;
130         5 0 2;
131         6 0 2;
132     ];
133
134     legendText = [...
135         '0.01g',
136         '0.20g',
137         '0.75g',
138         '1.00g'
139     ];
140
141     titleText = ['Frequency Response Function — Single isolator + 50 lbs, undamped, ver
142     return;
143
144 case 8
145     display = [...
146         22 1 2;
147         19 1 2;
148         20 1 2;
149         17 1 2;
150         18 1 2;
151     ];
152
153     legendText = [...
```

```
154         'No Damping',
155         'Neoprene damping, loose bolts',
156         'Neoprene damping, tight bolts',
157         'Buna N damping, loose bolts',
158         'Buna N damping, tight bolts'
159     ];
160 
161     titleText = ['Frequency Response Function — Single isolator + 30 lbs, damping compa
162     return;
163 
164 case 9
165     display = [...
166         40 3 4;
167         41 3 4;
168         42 3 4;
169         43 3 4;
170     ];
171 
172     legendText = [...
173         '0.03g Isolator C',
174         '0.05g Isolator C',
175         '0.075g Isolator C',
176         '0.1g Isolator C'
177     ];
178 
179     titleText = ['Frequency Response Function — Breadboard + 50 lbs, damped, lateral'];
180     return;
181 
182 case 10
183     display = [...
184         37 3 4;
185         41 3 4;
186     ];
187 
188     legendText = [...
189         '0.05g Undamped',
190         '0.05g Damped'
191     ];
192 
193     titleText = ['Frequency Response Function — Breadboard + 50 lbs, lateral'];
194     return;
195 
196 case 11
197     display = [...
198         44 3 4;
199         45 3 4;
200         46 3 4;
201         47 3 4;
202     ];
203 
204     legendText = [...
```

```
205         '0.03g Isolator C',
206         '0.05g Isolator C',
207         '0.075g Isolator C',
208         '0.1g Isolator C'
209     ];
210 
211     titleText = ['Frequency Response Function — Breadboard + 50 lbs, damped, longitudin
212     return;
213 
214 case 12
215     display = [...
216         33 3 4;
217         45 3 4;
218     ];
219 
220     legendText = [...
221         '0.05g Undamped',
222         '0.05g Damped'
223     ];
224 
225     titleText = ['Frequency Response Function — Breadboard + 50 lbs, longitudinal'];
226     return;
227 
228 
229 case 13
230     display = [...
231         48 3 4;
232         49 3 4;
233         50 3 4;
234         51 3 4;
235     ];
236 
237     legendText = [...
238         '0.03g Isolator A',
239         '0.05g Isolator A',
240         '0.075g Isolator A',
241         '0.1g Isolator A'
242     ];
243 
244     titleText = ['Frequency Response Function — Breadboard + 50 lbs, damped, vertical']
245     return;
246 
247 case 14
248     display = [...
249         29 3 4;
250         49 3 4;
251     ];
252 
253     legendText = [...
254         '0.05g Undamped',
255         '0.05g Damped'
```

```
256     ];
257
258     titleText = ['Frequency Response Function – Breadboard + 50 lbs, vertical'];
259     return;
260
261 case 15
262     display = [...
263         53 0 4;
264         54 0 4;
265         55 0 4;
266         56 0 4;
267     ];
268
269     legendText = [...
270         '0.03g Damped',
271         '0.05g Damped',
272         '0.008g Damped',
273         '0.005g Damped',
274         'location', 'southwest'
275     ];
276
277     titleText = ['Frequency Response Function – Random Vibe – Breadboard + 50 lbs, damp
278     return;
279
280
281 otherwise
282     display = 0;
283     legendText = 0;
284     titleText = 0;
285     return;
286
287 end % switch
288
289 end
```

Appendix B. Fabrication Drawing Sets

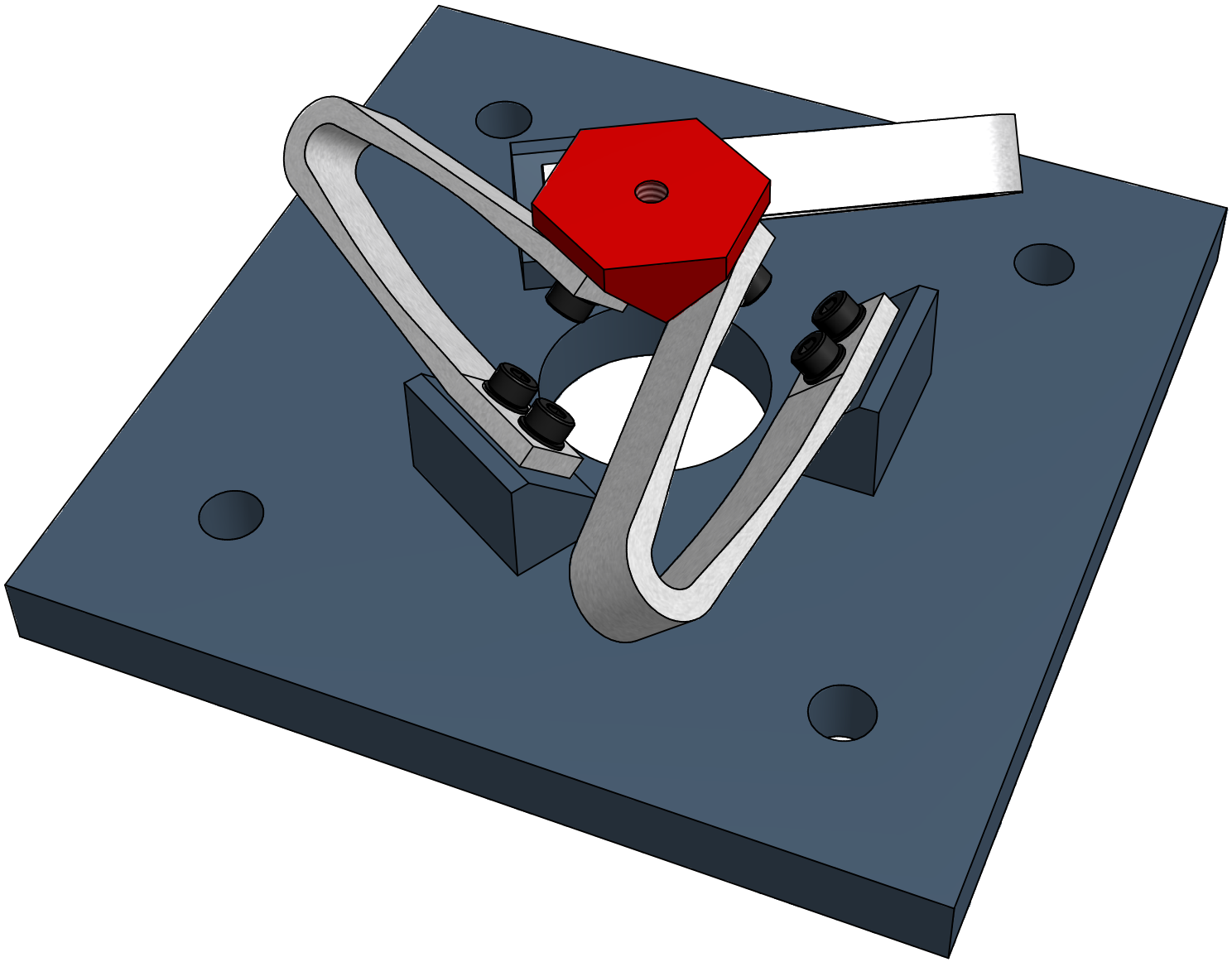

Triple Isolator Overview	
16 Dec 09	Triple Isolator
2d Lt Steven D. Miller	
steven.miller@afit.edu	
724-971-7225	

PRODUCED BY AN AUTODESK EDUCATIONAL PRODUCT
PRODUCED BY AN AUTODESK EDUCATIONAL PRODUCT
PRODUCED BY AN AUTODESK EDUCATIONAL PRODUCT

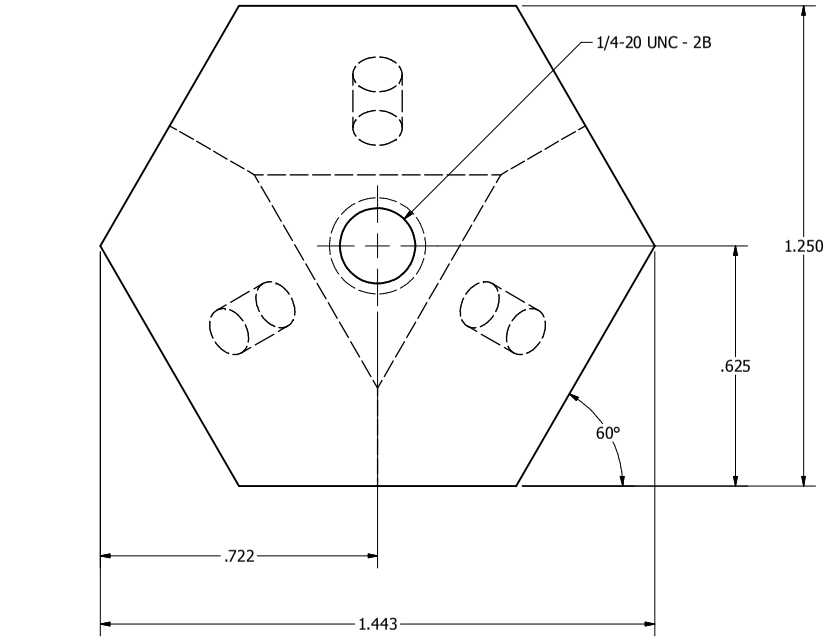

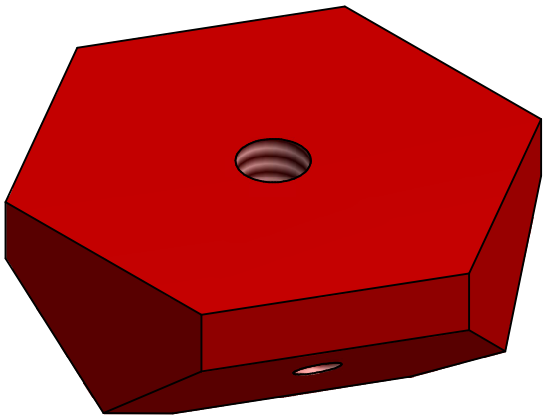

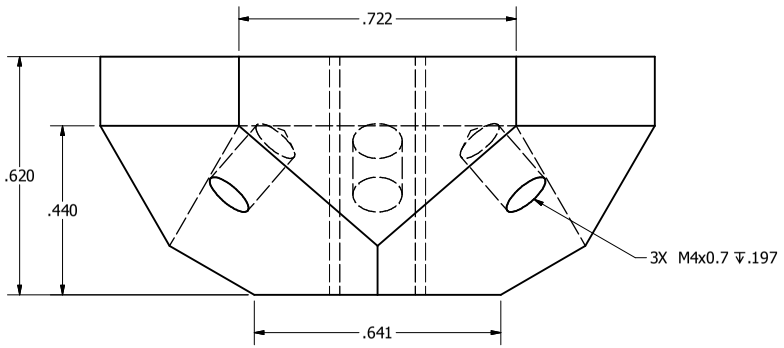

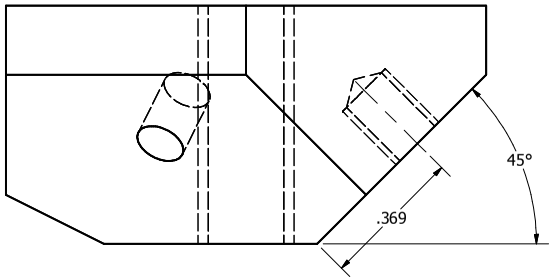

Jewel	
16 Dec 09	Triple Isolator
2d Lt Steven D. Miller	
steven.miller@afit.edu	
724-971-7225	

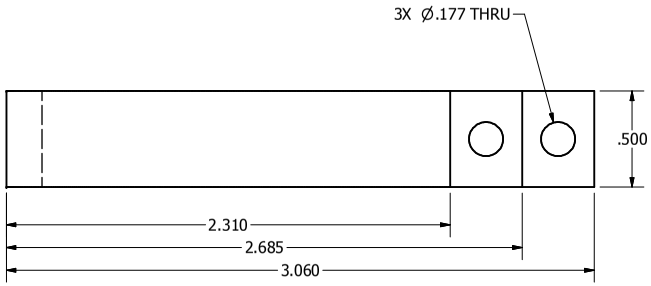

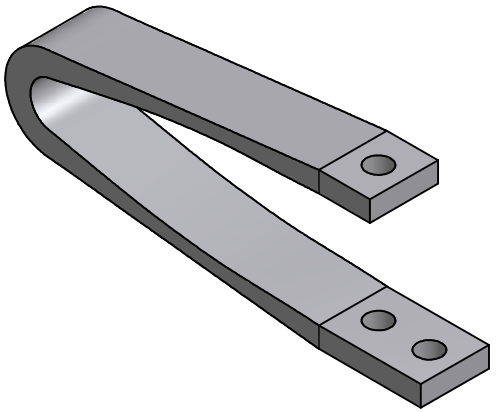

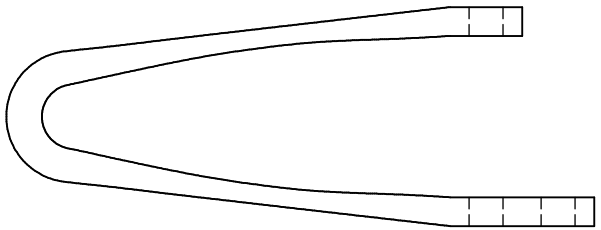

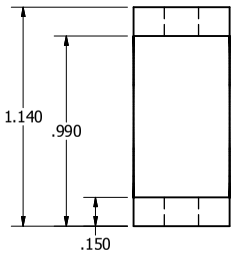

Spring	
16 Dec 09	Triple Isolator
2d Lt Steven D. Miller	
steven.miller@afit.edu	
724-971-7225	

PRODUCED BY AN AUTODESK EDUCATIONAL PRODUCT

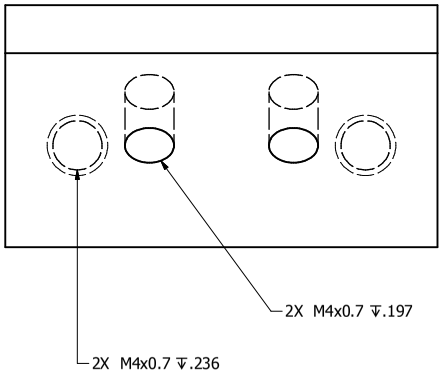

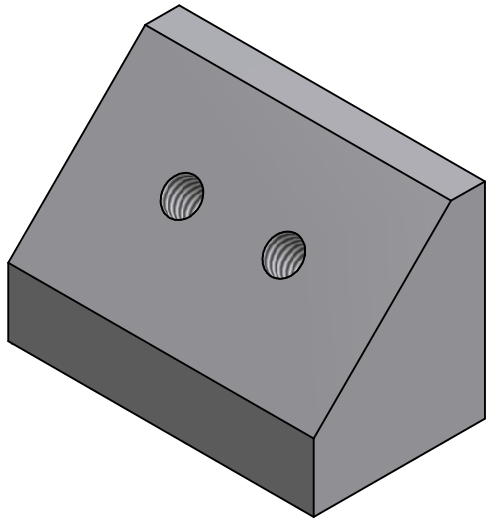

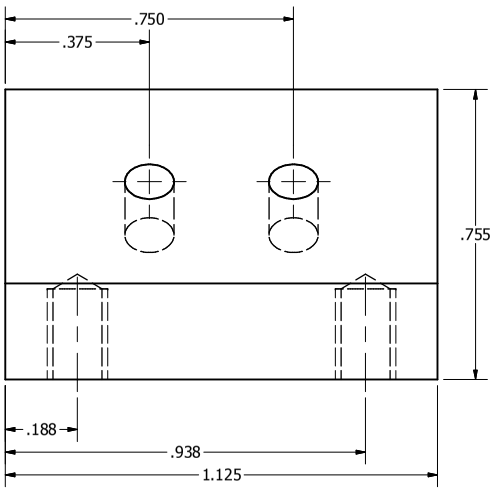

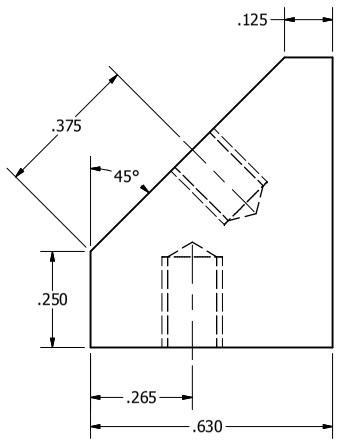

Support Post	
16 Dec 09	Triple Isolator
2d Lt Steven D. Miller	
steven.miller@afit.edu	
724-971-7225	

PRODUCED BY AN AUTODESK EDUCATIONAL PRODUCT

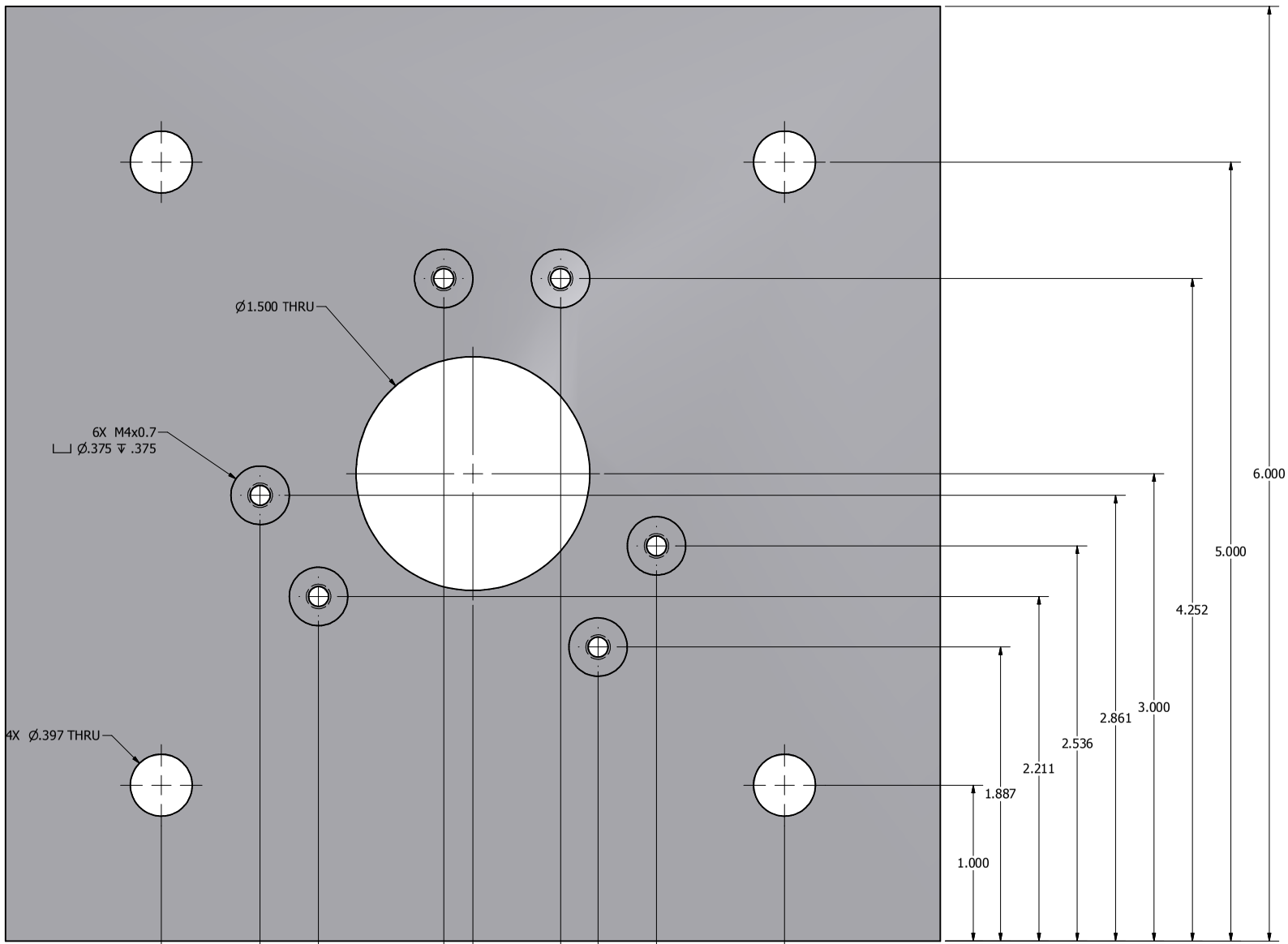

Base Plate	
16 Dec 09	Triple Isolator
2d Lt Steven D. Miller	
steven.miller@afit.edu	
724-971-7225	

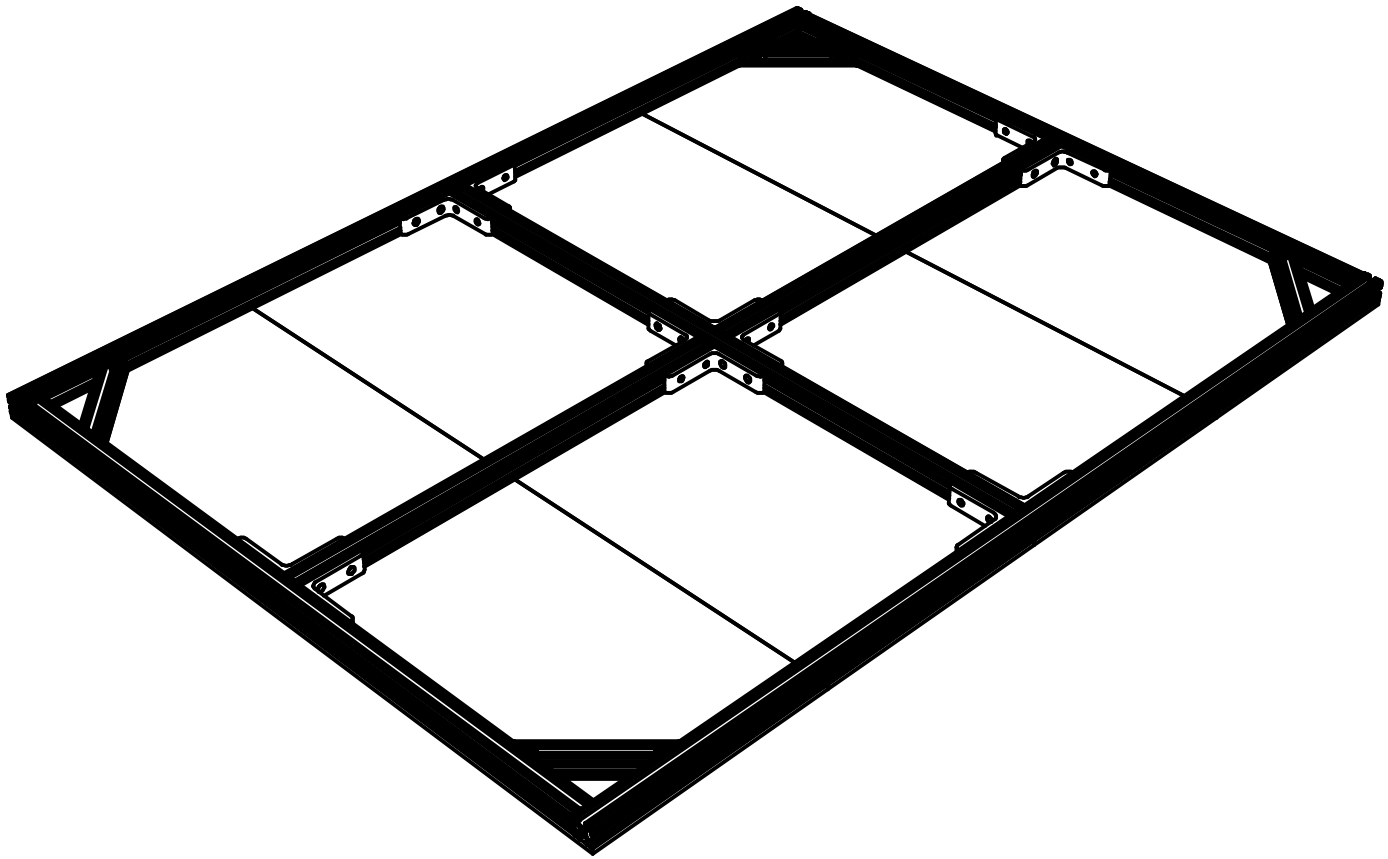

ISO Perspective
SCALE 0.12 : 1

NOTES:
1. Assembly weight = 96.7 lbs without attachment hardware (bolts, nuts, washers)
2. Top side aluminum plates not shown for clarity

RCOS Breadboard Sim	
30 Nov 09	CTEx
2d Lt Steven D. Miller	Sheet 1 of 3
steven.miller@afit.edu	
724-971-7225	

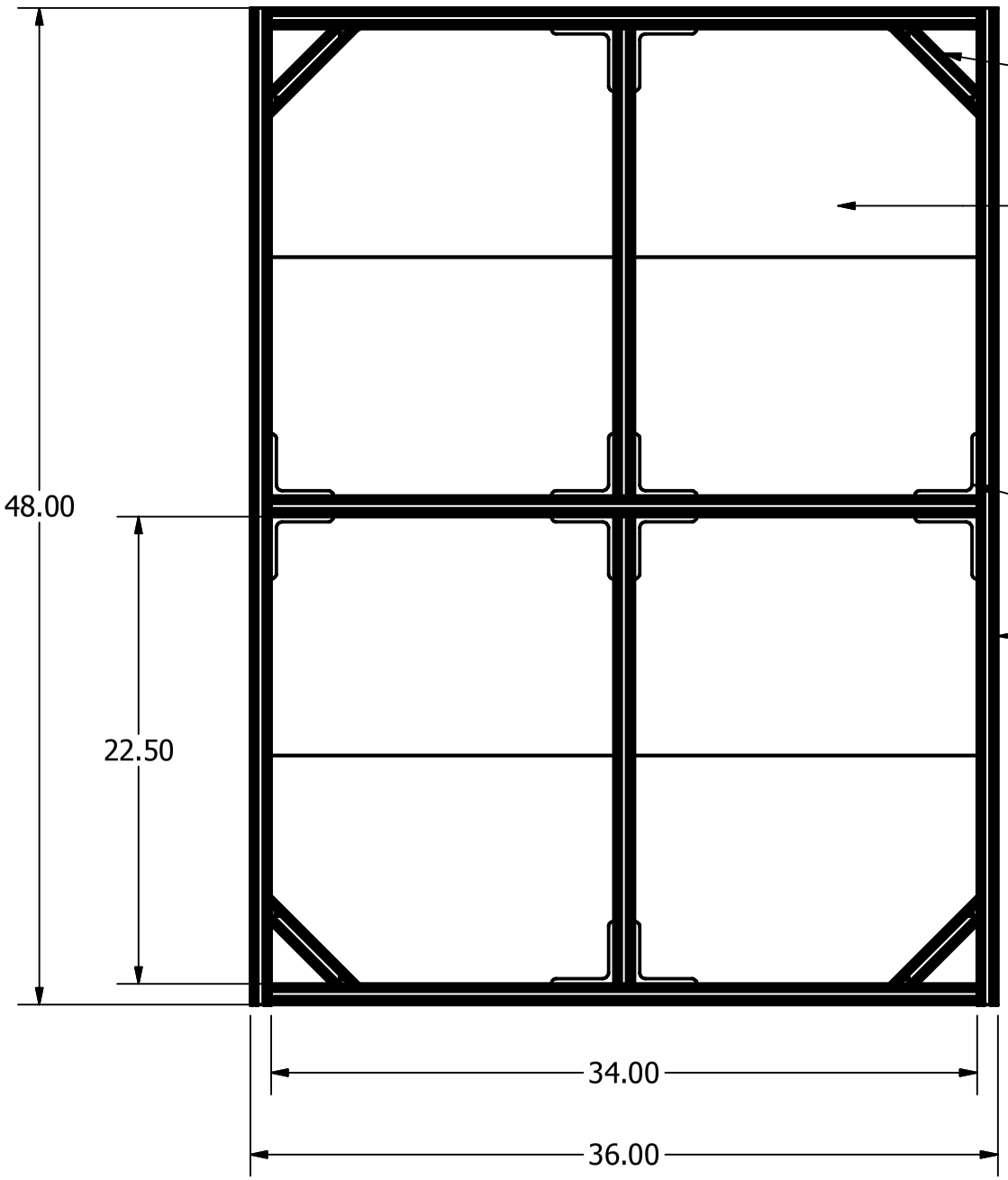

UNITS: Inch

RCOS Breadboard Sim	
30 Nov 09	CTEx
2d Lt Steven D. Miller	Sheet 2 of 3
steven.miller@afit.edu	
724-971-7225	

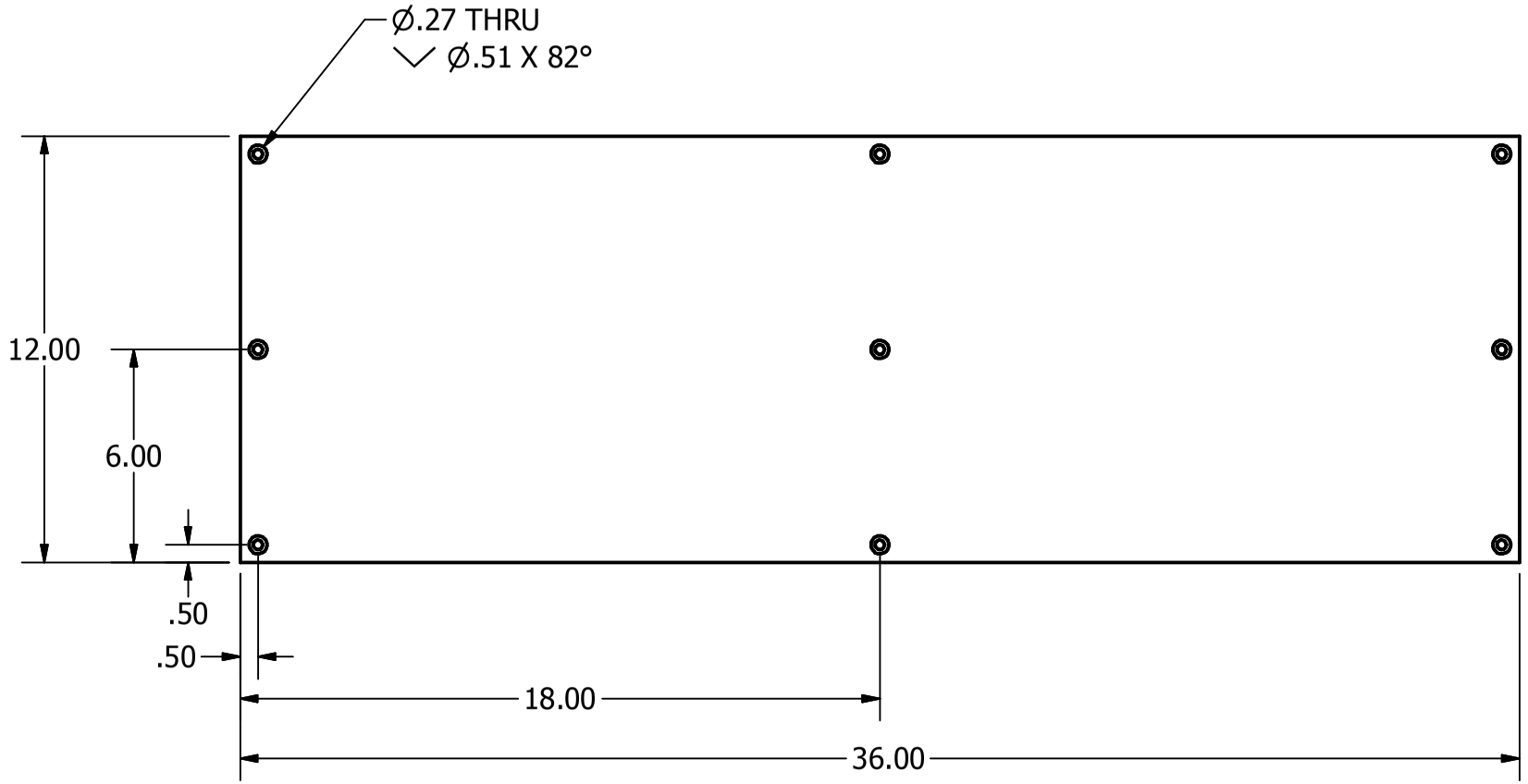

6061 Aluminum Plate
- 0.25 in thickness
- Shown with countersink for top plates
- Attach using 2 in 1/4-20 Flat Head Cap Screws
- Countersink flush with top plate, through hole in 80/20 and bottom plate
- Use flat washer and hex nut on back side
- Torque nuts to 30 in-lbs

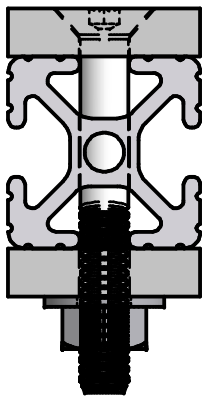

RCOS Breadboard Sim	
30 Nov 09	CTEx
2d Lt Steven D. Miller	Sheet 3 of 3
steven.miller@afit.edu	
724-971-7225	

Bibliography

1. Aeronautics, National and Space Administration, "International Space Station Imagery."
2. Agilent Technologies. *The Fundamentals of Modal Testing*, 2000. Application Note 243 - 3.
3. Anderson, Eric H., et al. *UltraQuiet Platform for Active Vibration Isolation*.
4. Bostick, Randall L. and Glen P. Perram. "Hyperspectral Imaging Using Chromotomography: A Fieldable Visible Instrument for Transient Events," *International Journal of High Speed Electronics and Systems* (2006).
5. Cobb, Richard G., et al. "Vibration Isolation and Suppression System for Precision Payloads in Space," *Smart Materials and Structures*, *8* (1999).
6. Cook, Robert D., et al. *Concepts and Applications of Finite Element Analysis* (Fourth Edition). John Wiley & Sons. Inc., 2002.
7. Daniel C. O'Dell, 1st Lt. Photograph, 2009. Air Force Institute of Technology.
8. Japan Aerospace Exploration Agency (JAXA). *Kibo HANDBOOK*, September 2007.
9. Johnson, Conor D., et al. *Protecting Satellites from the Dynamics of the Launch Environment*. 2004 S/C & L/V Dynamics Environments Workshop, June 2005.
10. MB Dynamics, Cleveland, OH. *C-Series "HP" Electro-Dynamic Shaker Systems*, February 2008.
11. National Space Development Agency of Japan (NASDA). *Introductory Guidebook for JEM Exposed Facility Potential Users*, 1998.
12. Taranti, Christian G. R., et al. "An Efficient Algorithm for Vibration Suppression to Meet Pointing Requirements of Optical Payloads," *American Institute of Aeronautics & Astronautics* (2001).

REPORT DOCUMENTATION PAGE

Form Approved
OMB No. 0704–0188

1. REPORT DATE (DD–MM–YYYY)	2. REPORT TYPE	3. DATES COVERED *(From — To)*
25-03-2010	Master's Thesis	15-12-2009 – 19-03-2010

4. TITLE AND SUBTITLE

Investigation of a Novel Compact Vibration Isolation System for Space Applications

5a. CONTRACT NUMBER

5b. GRANT NUMBER

5c. PROGRAM ELEMENT NUMBER

6. AUTHOR(S)

Steven D. Miller, 2d Lt, USAF

5d. PROJECT NUMBER

5e. TASK NUMBER

5f. WORK UNIT NUMBER

7. PERFORMING ORGANIZATION NAME(S) AND ADDRESS(ES)
Air Force Institute of Technology
Graduate School of Engineering and Management (AFIT/ENY)
2950 Hobson Way
WPAFB OH 45433-7765

8. PERFORMING ORGANIZATION REPORT NUMBER

AFIT/GA/ENY/10-M07

9. SPONSORING / MONITORING AGENCY NAME(S) AND ADDRESS(ES)

Undisclosed

10. SPONSOR/MONITOR'S ACRONYM(S)

11. SPONSOR/MONITOR'S REPORT NUMBER(S)

12. DISTRIBUTION / AVAILABILITY STATEMENT

APPROVED FOR PUBLIC RELEASE; DISTRIBUTION UNLIMITED

13. SUPPLEMENTARY NOTES

14. ABSTRACT

A novel compact vibration isolation system was designed, built, and tested for the Space Chromotomography Experiment (CTEx) being built by Air Force Institute of Technology (AFIT) researchers. CTEx is a multifunctional experimental imaging chromotomographic spectrometer designed for flight on the International Space Station (ISS) and is sensitive to jitter caused by vibrations both through the support structure as well as those produced on the optical platform by rotating optical components. CTEx demands a compact and lightweight means of vibration isolation and suppression from the ISS structure. Vibration tests conducted on an initial isolator design resulted in changes in the chosen spring and damping material properties but confirmed finite element (FE) model results and showed that the spring geometry meets preliminary design goals. The FE model served as a key tool in evaluating material and spring designs and development of the final drawing sets for fabrication. Research efforts led to a final design which was tested in the final flight configuration. This final configuration proved the potential for a compact means of vibration isolation for space applications.

15. SUBJECT TERMS

Vibration Isolation, Space Applications, Chromotomography Experiment

16. SECURITY CLASSIFICATION OF:			17. LIMITATION OF ABSTRACT	18. NUMBER OF PAGES	19a. NAME OF RESPONSIBLE PERSON
a. REPORT	b. ABSTRACT	c. THIS PAGE	UU	82	Eric Swenson, Lt Col, USAF
U	U	U			19b. TELEPHONE NUMBER (Include Area Code) (937)255-3636, x4749